博士論文

回転する弾性体の動的接触問題の変分法に基づく数値的取り扱いについて

(Numerical scheme for a dynamical rolling elastic contact problem based on a variational method)

金沢大学大学院自然科学研究科

数物科学専攻

学籍番号：1424012001

氏名：赤川佳穂

主任指導教員：小俣正朗

提出年月：2019年3月

Abstract

We investigate a rolling contact problem in elastodynamics. Contact problems in elasticity appear in various fields such as manufacturing and earthquake engineering. In particular, we have in mind the application to printers, where paper sheets are driven through the printer by rollers. A typical problem for such printers is that the roller may produce a squeaking sound. As a step towards preventing such a sound, we study a simplified model in which the roller is modeled as an elastic body driven by a rotation. The paper sheet is modeled as a rigid obstacle. For simplicity, we assume no frictional forces between the roller and the obstacle. The resulting equations of motion are of hyperbolic type with a free boundary.

The aim of the paper is to develop a numerical scheme to solve these equations of motion. The scheme is based on a variational method called the discrete Morse flow. The novelty is that this scheme has not been applied to a hyperbolic system with a free boundary where the unknown function is vector-valued.

Contents

Chapter 1

Introduction

Rolling contact problems appear throughout manufacturing wherever gears and tires are involved. We focus on the application to printers, where the rolling contact occurs at the place where the paper sheets are taken inside the printer (sheet feeder). The sheet feeder consists of rubber rollers which move the paper sheets through the printer. The problem with such sheet feeders is that they may produce a squeaking sound. This sound is caused by the contact of the rubber rollers with the paper sheets. In this paper, we work towards solving the problem of this squeaking sound by modeling the dynamics of the rubber rollers by elastodynamics.

Several earlier attempts have been made to model the dynamics of rollers. The first simplified model is introduced by Signorini [26], who models the rollers as static, linear elastic bodies subjected to a frictionless rigid obstacle. The Signorini problem was formulated and analyzed mathematically by [18] as a variational problem. To allow for large deformations, this model was extended to nonlinear elasticity and analyzed numerically by [16, 10]. There, the authors studied the equations for the steady state of a rolling hyperelastic material in contact with an obstacle by Coulomb friction, and implemented a numerical scheme for it. However, the steady-state solutions cannot explain the squeaking sound. It remains difficult to solve the rolling contact problem by using the equation of elastodynamics, because the related set of equations contain a free boundary, are of hyperbolic nature, and are nonlinear due to the use of hyperelasticity to allow for large deformations.

Therefore our aim is to extend the numerical scheme for the stationary setting in [16, 10] to a dynamical scheme. Since it is difficult to treat at once the free boundary, hyperbolic dynamics and the nonlinearities that come with hyperelasticity, we will use instead the equations of linear elasticity in the coordinate frame which rotates along with the roller. The resulting equations are of hyperbolic type with a free boundary.

Our numerical scheme is based on the discrete Morse flow (DMF), which was introduced by [13]. The DMF is a variational method based on a minimizing movement scheme which was intended for parabolic type problems. [30] extended the application of the DMF to problems of hyperbolic type. [16] further extended it such that hyperbolic problems with free boundaries can be treated. The key idea is to put the obstacle constraint as a restriction on the admissible set over which the energy functional related to the DMF is minimized.

However, [16] treats the case of scalar-valued functions, while the application of the DMF to our setting requires the extension to vector-valued functions. The aim of this paper is

therefore to extend the DMF to vector-valued functions. We demonstrate the use of this extension by applying it to a rolling contact problem.

In Chapter 2, we explain about the variational structure of a stationary obstacle problem. Free boundary conditions appears on the contact zone. We suppose that the obstacle is frictionless and undeformed. This conditions are derived naturally from a variational problem.

In Chapter 3, we derive the set of model equations for the rolling contact problem. The deformation including rotation is treated as finite deformation. In the finite deformation the nonlinear elasticity appears, it is not easy to treat. We suppose reasonable assumption that the deformation is decomposed with rotation and small displacement since the object is rubber roller. From this decompose assumption, we describe the original nonlinear elasticity equations as a linear elasticity equations for the small displacement. On the other hand, the obtained equation is a linear elasticity equation with a outer force coming from the rotation effects. In §3.3, we discuss the preserving of the model equations. In §3.4, we discuss the boundary conditions including free boundary conditions coming from obstacle. We suppose that the obstacle is frictionless and undeformed. These free boundary conditions are derived naturally from the variational structure. We explain the detail of it in §4.2 as the time discretized form.

In Chapter 4, we suggest a variant of the discrete Morse flow to develop a numerical scheme in which the total energy preserves for the vibration of the small displacement. The proposed time discrete scheme haves $O(\Delta t^2)$–accuracy for the acceleration part, but the oder of the approximation of the outer force is $O(\Delta t)$. It is not satisfactory. We show the existence of the minimizer of the employed time-discretized type functional in §4.3. However we have not prove the convergence of the approximate solution interpolated in time by the minimizers. In §4.4, we explain a variant of the nonlinear conjugate gradient method. The elasticity is linear however the problem is nonlinear since it contains free boundary condition coming from the obstacle. Hence we employ the nonlinear conjugate gradient method. Moreover we need to make it a variant type because of the constraint. To constrain the obstacle in nonlinear conjugate gradient method, we use the orthogonal projection onto the admissible set, and operator which restricts the search direction as as not to jump over the obstacle.

In Chapter 5, we solve time discretized problem numerically and discuss the application to the rolling contact problem. We simulate two cases. In the first case we remove the obstacle, and study the sensitivity of the roller's dynamics with respect to the parameters. In particular, we are interested in the vibrations in the radial and tangential displacements, because the understanding of these vibrations might help in removing the squeaking sound of printer rollers. In the second case we add the obstacle. We are interested in the shape of the deformed domain and the size of the stress tensor, especially in the region close to the contact zone.

In Chapter 6, we we explain the details of the discrete Morse flow for a linear elasticity problem. The discrete Morse flow method is a method which constructs a weak solution by the limit function of the approximate solution interpolated in time with minimizers of a time-discretized type functionals over an admissible set. The steps of the construction of a weak solution is as follows: (i) Show the existence of a minimizer of the time-discretized type functional over the admissible set, and construct an approximate solution. (ii) Show the boundedness of the approximate solution sequence, and construct weakly converging

subsequence by theorem by Eberlein and Shmulyan. (iii) Show that the limit of the sequence is weak solution. It is useful to describe the free boundary condition only by restricting the admissible set. In our model case, the free boundary condition is corresponding to the obstacle which is frictionless and undeformed. In this Chapter, using a simple case that linear elasticity problem with homogeneous Dirichlet boundary without constraint, we explain the details of the discrete Morse flow. On the other hand, this method is possible to apply the finite element method as a numerical method. When we treat a admissible set, a variant of the nonlinear conjugate gradient method with a projection may be possible to solve a minimizing problem numerically.

Chapter 2

Obstacle problem

2.1 Geometry

Let $\Omega \subset \mathbb{R}^2$ be a bounded domain representing the area occupied by an elastic body. The closure $\overline{\Omega}$ of the set Ω is called the reference configuration. We subdivide the boundary $\partial\Omega$ into Γ_D and Γ_C, where

$$\Gamma_D \cup \Gamma_C = \partial\Omega, \quad \Gamma_D \cap \Gamma_C = \emptyset, \quad \Gamma_D \neq \emptyset. \tag{2.1}$$

We denote by $\boldsymbol{u} : \overline{\Omega} \to \mathbb{R}^2$ the displacement of the reference configuration $\overline{\Omega}$. We introduce the strain tensor

$$\boldsymbol{\epsilon}[\boldsymbol{u}] := \frac{1}{2}\left(\nabla \boldsymbol{u} + \nabla \boldsymbol{u}^T\right), \tag{2.2}$$

and the stress tensor

$$\boldsymbol{\sigma}[\boldsymbol{u}] := 2\mu\boldsymbol{\epsilon}[\boldsymbol{u}] + \lambda(\operatorname{div} \boldsymbol{u})\boldsymbol{I}. \tag{2.3}$$

where μ and λ are the Lamé constants ($\lambda + \mu \geq 0$, $\mu > 0$). We define the elasticity tensor

$$c_{ijpq} := \lambda\delta_{ij}\delta_{pq} + \mu(\delta_{ip}\delta_{jq} + \delta_{iq}\delta_{jp}). \tag{2.4}$$

Using (2.4) we rewrite (2.3) by

$$\sigma_{ij} = c_{ijpq}\epsilon_{pq} \tag{2.5}$$

Here and henceforth we use the convention to sum over repeated indices.

Then the elasticity tensor c_{ijpq} satisfies the following properties:

(1) $c_{ijpq} = c_{jipq} = c_{pqij}$,

(2) $c_{ijpq}\epsilon_{pq}\epsilon_{ij} \geq 2\mu\epsilon_{ij}\epsilon_{ij}$,

(3) $c_{ijpq}\epsilon_{pq}[\boldsymbol{u}]\epsilon_{ij}[\boldsymbol{u}] = c_{ijpq}\dfrac{\partial u_p}{\partial x_q}\dfrac{\partial u_i}{\partial x_j}$.

Indeed, we can get (1) and (2) easily. Proof of (3), using the symmetries (1) we obtain

$$\begin{aligned} c_{ijpq}\epsilon_{pq}[\boldsymbol{u}]\epsilon_{ij}[\boldsymbol{u}] &= \frac{1}{4}c_{ijpq}\left(\frac{\partial u_p}{\partial x_q}+\frac{\partial u_q}{\partial x_p}\right)\left(\frac{\partial u_i}{\partial x_j}+\frac{\partial u_j}{\partial x_i}\right) \\ &= \frac{1}{4}\left(c_{ijpq}\frac{\partial u_p}{\partial x_q}\frac{\partial u_i}{\partial x_j}+c_{ijpq}\frac{\partial u_p}{\partial x_q}\frac{\partial u_j}{\partial x_i}+c_{ijpq}\frac{\partial u_q}{\partial x_p}\frac{\partial u_i}{\partial x_j}+c_{ijpq}\frac{\partial u_q}{\partial x_p}\frac{\partial u_i}{\partial x_j}\right) \\ &= \frac{1}{4}\left(c_{ijpq}+c_{jipq}+c_{ijqp}+c_{qpji}\right)\frac{\partial u_p}{\partial x_q}\frac{\partial u_i}{\partial x_j} \\ &= c_{ijpq}\frac{\partial u_p}{\partial x_q}\frac{\partial u_i}{\partial x_j}. \end{aligned}$$

We shall consider the following stationary obstacle problem in linear elasticity:

$$-\operatorname{\mathbf{div}}\boldsymbol{\sigma}[\boldsymbol{u}] = \mathbf{0} \qquad \text{in} \quad \Omega, \tag{2.6}$$

$$\boldsymbol{u} = \mathbf{0} \qquad \text{on} \quad \Gamma_D, \tag{2.7}$$

$$\big(\boldsymbol{\sigma}[\boldsymbol{u}]\boldsymbol{n}\big)_1 = 0 \qquad \text{on} \quad \Gamma_C, \tag{2.8}$$

$$\big(\mathbf{id}+\boldsymbol{u}\big)_2 \geq g \qquad \text{on} \quad \Gamma_C, \tag{2.9}$$

$$\big(\boldsymbol{\sigma}[\boldsymbol{u}]\boldsymbol{n}\big)_2 \geq 0 \qquad \text{on} \quad \Gamma_C, \tag{2.10}$$

$$\Big(\big(\mathbf{id}+\boldsymbol{u}\big)_2 - g\Big)\big(\boldsymbol{\sigma}[\boldsymbol{u}]\boldsymbol{n}\big)_2 = 0 \qquad \text{on} \quad \Gamma_C, \tag{2.11}$$

where $\boldsymbol{n}$ is unit outer normal vector of $\partial\Omega$. The condition (2.8) tells free slip. The condition (2.9) means that the position should be above from obstacle. The condition (2.10) describes that normal components must be compressive. Summarizing (2.9)–(2.11), it means that at least one of (2.9) and (2.10) holds equality.

For equation (2.6)–(2.11), we consider the minimizing the functional

$$\mathcal{E}(\boldsymbol{u}) := \frac{1}{2}\int_\Omega \boldsymbol{\sigma}[\boldsymbol{u}] : \boldsymbol{\epsilon}[\boldsymbol{u}]\,dx \tag{2.12}$$

over to the admissible set

$$\mathcal{K} := \left\{\boldsymbol{u}\in W^{1,2}(\Omega;\mathbb{R}^2);\ \boldsymbol{u}=\mathbf{0} \text{ a.e. on } \Gamma_D,\ (\mathbf{id}+\boldsymbol{u})_2 \geq g \text{ a.e. on } \Gamma_C\right\}. \tag{2.13}$$

Here, $\boldsymbol{\sigma} : \boldsymbol{\epsilon} := \sigma_{ij}\epsilon_{ij}$. By calculating the first variation of $\mathcal{E}$ over $\mathcal{K}$, we obtain that any minimizer satisfies (2.6)–(2.11). The existence of a unique minimizer follows from the facts that $\mathcal{E}$ is weakly lower semi–continuous on $W^{1,2}(\Omega;\mathbb{R}^2)$, is bounded from below, has bounded sublevel sets, and that $\mathcal{K}$ is convex and closed in $W^{1,2}(\Omega;\mathbb{R}^2)$ (see §4.3 for the details).

Let us check that the sufficiently smooth minimizer $\boldsymbol{u}$ satisfies (2.6)–(2.11) by the analogy of [9]. The minimizer $\boldsymbol{u}$ satisfies the inequality

$$\mathcal{E}(\boldsymbol{v}) \geq \mathcal{E}(\boldsymbol{u}) \qquad \text{for all } \boldsymbol{v}\in\mathcal{K}.$$

Taking any $\boldsymbol{w}\in C^\infty(\overline{\Omega};\mathbb{R}^2)$ such that $\boldsymbol{v}=\boldsymbol{u}+s\boldsymbol{w}\in\mathcal{K}$ for small $s\geq 0$, expanding $\mathcal{E}(\boldsymbol{u}+s\boldsymbol{w})$

in terms of s, we deduce that the first-order term in s must be non-negative, that is,

$$\begin{aligned} 0 &\leq \mathcal{E}(\boldsymbol{u} + s\boldsymbol{w}) - \mathcal{E}(\boldsymbol{w}), \\ 0 &\leq \frac{1}{s}\left(\mathcal{E}(\boldsymbol{u} + s\boldsymbol{w}) - \mathcal{E}(\boldsymbol{w})\right), \\ 0 &\leq \frac{d}{ds}\mathcal{E}(\boldsymbol{u} + s\boldsymbol{w})\Big|_{s=0} \\ &= \int_\Omega \boldsymbol{\sigma}[\boldsymbol{u}] : \boldsymbol{\epsilon}[\boldsymbol{w}]\, dx. \end{aligned}$$

Integrating by parts, we have

$$0 \leq -\int_\Omega \mathbf{div}\, \boldsymbol{\sigma}[\boldsymbol{u}] \cdot \boldsymbol{w}\, dx + \int_{\Gamma_C} (\boldsymbol{\sigma}[\boldsymbol{u}]\boldsymbol{n}) \cdot \boldsymbol{w}\, dx \tag{2.14}$$

Choosing $\boldsymbol{w} \in C_0^\infty(\Omega; \mathbb{R}^2)$, (2.14) implies (2.6). Thus for $\boldsymbol{w} \in C^\infty(\overline{\Omega}; \mathbb{R}^2)$, we deduce from (2.14)

$$0 \leq \int_{\Gamma_C} (\boldsymbol{\sigma}[\boldsymbol{u}]\boldsymbol{n}) \cdot \boldsymbol{w}\, ds \tag{2.15}$$

If we choose $\boldsymbol{w}$ such that

$$w_2 = 0 \quad \text{ on } \Gamma_C,$$

we deduce (2.8). And if we choose a function $\boldsymbol{w}$ such that

$$w_2 \geq 0 \quad \text{ on } \Gamma_C,$$

then $\boldsymbol{v} = \boldsymbol{u} + s\boldsymbol{v} \in \mathcal{K}$ for small $s \geq 0$ and (2.15) yields (2.10) Finally, suppose that $(\mathbf{id} + \boldsymbol{u})_2 - g > 0$ at a point $\boldsymbol{x} \in \Gamma_C$. Then there exists $\boldsymbol{w} \in C^\infty(\overline{\Omega}; \mathbb{R}^2)$ such that

$$w_2(\boldsymbol{x}) < 0 \quad \text{ and } \quad (\mathbf{id} + \boldsymbol{u} + s\boldsymbol{w})_2 - g \geq 0 \quad \text{ on } \Gamma_C \text{ for small } s \geq 0.$$

Condition (2.15) together with (2.10) implies

$$\Big(\big(\mathbf{id} + \boldsymbol{u}\big)_2 - g\Big)\big(\boldsymbol{\sigma}[\boldsymbol{u}]\boldsymbol{n}\big)_2 = 0$$

and therefore (2.11) holds.

Chapter 3

Rolling contact problem

In this section, we introduce our notation and the set of governing equations (P).

3.1 Geometry

Let $\Omega \subset \mathbb{R}^2$ be a bounded domain representing the area occupied by an elastic body. The closure $\overline{\Omega}$ of the set Ω is called the reference configuration. We denote by $\boldsymbol{\varphi} : \overline{\Omega} \to \mathbb{R}^2$ the deformation of the reference configuration $\overline{\Omega}$, and refer to $\boldsymbol{\varphi}(\overline{\Omega})$ as the deformed configuration. We call the components of $\boldsymbol{x}$ the Lagrangian coordinates, and the components of $\boldsymbol{X} = \boldsymbol{\varphi}(\boldsymbol{x})$ the Eulerian coordinates (see Figure 3.1) in the deformed configuration.

At each point $\boldsymbol{x} \in \Omega$, the deformation gradient is given by

$$\boldsymbol{F}(\boldsymbol{x}) := \nabla \boldsymbol{\varphi}(\boldsymbol{x}) = \begin{pmatrix} \dfrac{\partial \varphi_1}{\partial x_1}(\boldsymbol{x}) & \dfrac{\partial \varphi_1}{\partial x_2}(\boldsymbol{x}) \\ \dfrac{\partial \varphi_2}{\partial x_1}(\boldsymbol{x}) & \dfrac{\partial \varphi_2}{\partial x_2}(\boldsymbol{x}) \end{pmatrix}. \tag{3.1}$$

We require that the determinant of the deformation gradient is positive at all points of the reference configuration, that is

$$J(\boldsymbol{x}) := \det \boldsymbol{F}(\boldsymbol{x}) > 0, \tag{3.2}$$

for all $\boldsymbol{x} \in \Omega$. As a consequence, the matrix $\boldsymbol{F}(\boldsymbol{x})$ is invertible.

Before linearizing, we describe the equations for mechanical equilibrium in terms of nonlinear elasticity. The Cauchy stress tensor $\boldsymbol{T} = (T_{ij})$ is defined in the deformed configuration

$$\boldsymbol{T}(\boldsymbol{X}) := \frac{1}{J(\boldsymbol{x})} \left\{ \mu \left(\boldsymbol{F}(\boldsymbol{x}) \boldsymbol{F}^T(\boldsymbol{x}) - \boldsymbol{I} \right) + \frac{\lambda}{2} \left(J(\boldsymbol{x})^2 - 1 \right) \boldsymbol{I} \right\}, \tag{3.3}$$

for all $\boldsymbol{x} \in \Omega$, where $\boldsymbol{X} = \boldsymbol{\varphi}(\boldsymbol{x})$, μ and λ are the Lamé constants ($\lambda + \mu \geq 0$, $\mu > 0$), $\boldsymbol{F}^T(\boldsymbol{x})$ is the transpose matrix of $\boldsymbol{F}(\boldsymbol{x})$, and $\boldsymbol{I}$ is the identity matrix.

In our model for the roller, the deformation naturally decomposes as

$$\boldsymbol{\varphi} = \boldsymbol{R}(\mathbf{id} + \boldsymbol{\xi}) \quad \text{in } \Omega, \tag{3.4}$$

where the matrix $\boldsymbol{R} = (R_{ij})$ describes the counter-clockwise rotation by angle θ (see Figure 3.1), $\mathbf{id} : \mathbb{R}^2 \to \mathbb{R}^2$ denotes the identity map, and $\boldsymbol{\xi} : \Omega \to \mathbb{R}^2$ is assumed to have small derivatives. More precisely, we assume that

$$\left|\frac{\partial \xi_i}{\partial x_j}(\boldsymbol{x})\right| < \varepsilon, \qquad \left|\frac{\partial^2 \xi_i}{\partial x_j \partial \xi_k}(\boldsymbol{x})\right| < \varepsilon, \tag{3.5}$$

for some $\varepsilon > 0$ small enough, uniformly for $\boldsymbol{x} \in \Omega$ and $1 \le i, j, k \le 2$.

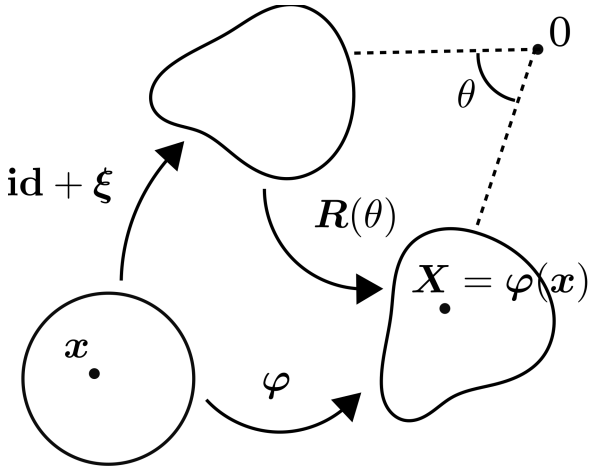

Figure 3.1: Sketch of the decomposition of the deformation $\boldsymbol{\varphi}$.

3.2 Equations of motion

To derive the equations of motion, we change variables in (3.3) by writing it in terms of $\boldsymbol{\xi}$ on Ω, and expand it in terms of ε by relying on (3.5). Since $\nabla\boldsymbol{\xi}$ plays the role of the deformation in linearized elasticity, we introduce the strain tensor

$$\boldsymbol{\epsilon}[\boldsymbol{\xi}] := \frac{1}{2}\left(\nabla\boldsymbol{\xi} + \nabla\boldsymbol{\xi}^T\right), \tag{3.6}$$

and the stress tensor

$$\boldsymbol{\sigma}[\boldsymbol{\xi}] := 2\mu\boldsymbol{\epsilon}[\boldsymbol{\xi}] + \lambda(\operatorname{div}\boldsymbol{\xi})\boldsymbol{I}, \tag{3.7}$$

in the reference configuration. The Cauchy stress tensor $\boldsymbol{T}(\boldsymbol{X})$ in Lagrangian coordinates is given as

$$\begin{aligned}
T_{ij} &= \frac{1}{J}\left\{\mu\left[R_{ik}\left(\delta_{k\ell} + \frac{\partial \xi_k}{\partial x_\ell}\right)\left(\delta_{m\ell} + \frac{\partial \xi_m}{\partial x_\ell}\right)R_{jm} - \delta_{ij}\right] + \frac{\lambda}{2}\left[\Big(1 + \operatorname{div}\boldsymbol{\xi} + \det(\nabla\boldsymbol{\xi})\Big)^2 - 1\right]\delta_{ij}\right\} \\
&= \frac{1}{J}\left\{\mu R_{ik}\left(\frac{\partial \xi_k}{\partial x_m} + \frac{\partial \xi_m}{\partial x_k} + \frac{\partial \xi_k}{\partial x_\ell}\frac{\partial \xi_m}{\partial x_\ell}\right)R_{jm}\right. \\
&\quad \left. + \frac{\lambda}{2}\left[2\Big(\operatorname{div}\boldsymbol{\xi} + \det(\nabla\boldsymbol{\xi})\Big) + \Big(\operatorname{div}\boldsymbol{\xi} + \det(\nabla\boldsymbol{\xi})\Big)^2\right]R_{ik}\delta_{km}R_{jm}\right\} \\
&= \frac{1}{J}R_{ik}\sigma_{km}[\boldsymbol{\xi}]R_{jm} + \frac{1}{J}R_{ik}\left\{\mu\frac{\partial \xi_k}{\partial x_\ell}\frac{\partial \xi_m}{\partial x_\ell} + \frac{\lambda}{2}\left[2\det(\nabla\boldsymbol{\xi}) + \Big(\operatorname{div}\boldsymbol{\xi} + \det(\nabla\boldsymbol{\xi})\Big)^2\right]\delta_{km}\right\}R_{jm}.
\end{aligned}$$

Here and henceforth we use the convention to sum over repeated indices. The divergence of the tensor $\boldsymbol{T}$ is then

$$\begin{aligned}(\mathbf{div}_{\mathrm{X}}\,\boldsymbol{T})_i := \frac{\partial T_{ij}}{\partial X_j} &= R_{ik}\left(\frac{1}{J}\frac{\partial}{\partial x_m}\sigma_{k\ell}[\boldsymbol{\xi}] - \frac{1}{J^2}\sigma_{k\ell}[\boldsymbol{\xi}]\frac{\partial J}{\partial x_m}\right)\frac{\partial(\boldsymbol{\varphi}^{-1})_m}{\partial x_j}R_{j\ell} + O(\varepsilon^2)\\ &= R_{ik}\left(1 - \Big(\operatorname{div}\boldsymbol{\xi} + \det(\nabla\boldsymbol{\xi})\Big) + O(\varepsilon^2)\right)\frac{\partial}{\partial x_m}\sigma_{k\ell}[\boldsymbol{\xi}]R_{jm}R_{j\ell} + O(\varepsilon^2)\\ &= R_{ik}\frac{\partial}{\partial x_\ell}\sigma_{k\ell}[\boldsymbol{\xi}] + O(\varepsilon^2),\end{aligned} \tag{3.8}$$

where $\boldsymbol{\varphi}^{-1}$ is the inverse function of $\boldsymbol{\varphi}$.

Next we derive the equations of motion. We encode the forced rotation of the elastic body by a given smooth function $\theta : [0,T) \to \mathbb{R}$ that corresponds to the rotation angle of $\boldsymbol{R}$. Then, by (3.4), the now time-dependent fields $\boldsymbol{\varphi} : \overline{\Omega} \times [0,T) \to \mathbb{R}^2$ and $\boldsymbol{\xi} : \overline{\Omega} \times [0,T) \to \mathbb{R}^2$ satisfy

$$\boldsymbol{\varphi}(\boldsymbol{x},t) = \boldsymbol{R}(\theta(t))(\boldsymbol{x} + \boldsymbol{\xi}(\boldsymbol{x},t)), \tag{3.9}$$

for all $\boldsymbol{x} \in \overline{\Omega}$ and all $t \geq 0$. After neglecting higher order terms of ε in (3.8), the conservation of linear momentum yields the equation of elastodynamics,

$$\rho\ddot{\boldsymbol{\varphi}} = \mathbf{div}_{\boldsymbol{X}}\,\boldsymbol{T} \approx \boldsymbol{R}(\theta)\,\mathbf{div}\,\boldsymbol{\sigma}[\boldsymbol{\xi}] \quad \text{in } \Omega \times (0,T), \tag{3.10}$$

where $\rho > 0$ is the density, superposed dots denote partial differentiation with respect to time (i.e., $\ddot{\boldsymbol{\varphi}} := \partial^2\boldsymbol{\varphi}/\partial t^2$), and

$$\mathbf{div}\,\boldsymbol{\sigma} := \begin{pmatrix} \dfrac{\partial\sigma_{11}}{\partial x_1} + \dfrac{\partial\sigma_{12}}{\partial x_2} \\ \dfrac{\partial\sigma_{21}}{\partial x_1} + \dfrac{\partial\sigma_{22}}{\partial x_2} \end{pmatrix}. \tag{3.11}$$

To write the left hand side of (3.10) in terms of $\boldsymbol{\xi}$, we use (3.9) to compute

$$\begin{aligned}\ddot{\boldsymbol{\varphi}} &= \ddot{\theta}\frac{d}{d\theta}\boldsymbol{R}(\theta)(\mathbf{id}+\boldsymbol{\xi}) + \dot{\theta}^2\frac{d^2}{d\theta^2}\boldsymbol{R}(\theta)(\mathbf{id}+\boldsymbol{\xi}) + 2\dot{\theta}\frac{d}{d\theta}\boldsymbol{R}(\theta)\dot{\boldsymbol{\xi}} + \boldsymbol{R}(\theta)\ddot{\boldsymbol{\xi}}\\ &= \boldsymbol{R}(\theta)\left\{\ddot{\theta}\boldsymbol{R}(\pi/2)(\mathbf{id}+\boldsymbol{\xi}) + \dot{\theta}^2\boldsymbol{R}(\pi)(\mathbf{id}+\boldsymbol{\xi}) + 2\dot{\theta}\boldsymbol{R}(\pi/2)\dot{\boldsymbol{\xi}} + \ddot{\boldsymbol{\xi}}\right\}\\ &= \boldsymbol{R}(\theta)\left\{-\ddot{\theta}\boldsymbol{R}(-\pi/2)(\mathbf{id}+\boldsymbol{\xi}) - \dot{\theta}^2(\mathbf{id}+\boldsymbol{\xi}) - 2\dot{\theta}\boldsymbol{R}(-\pi/2)\dot{\boldsymbol{\xi}} + \ddot{\boldsymbol{\xi}}\right\}.\end{aligned}$$

In the above calculation, we have used that $\frac{d}{d\theta}\boldsymbol{R}(\theta) = \boldsymbol{R}(\theta)\boldsymbol{R}(\pi/2)$. Inserting the result in (3.10), we obtain

$$\rho\ddot{\boldsymbol{\xi}} = \mathbf{div}\,\boldsymbol{\sigma}[\boldsymbol{\xi}] + \rho\left(\ddot{\theta}\boldsymbol{R}(-\pi/2)(\mathbf{id}+\boldsymbol{\xi}) + \dot{\theta}^2(\mathbf{id}+\boldsymbol{\xi}) + 2\dot{\theta}\boldsymbol{R}(-\pi/2)\dot{\boldsymbol{\xi}}\right) \quad \text{in } \Omega\times(0,T). \tag{3.12}$$

We note that if θ is linear in time, then in the right-hand side the second term vanishes, the third term is the centrifugal force, and the last term is the Coriolis force. To abbreviate the term in parentheses, we define the function $\boldsymbol{f}$ by

$$\boldsymbol{f}(t,\boldsymbol{x},\boldsymbol{\xi},\dot{\boldsymbol{\xi}}) := \ddot{\theta}(t)\boldsymbol{R}(-\pi/2)(\boldsymbol{x}+\boldsymbol{\xi}) + \dot{\theta}(t)^2(\boldsymbol{x}+\boldsymbol{\xi}) + 2\dot{\theta}(t)\boldsymbol{R}(-\pi/2)\dot{\boldsymbol{\xi}}. \tag{3.13}$$

We remark that the time dependence of the rotation angle is not covered by the setting in [21, 16].

3.3 Total energy

In this section, we discuss the preserving quantity of this model in the case with Dirichlet zero and Neumann zero boundary conditions. Therefore, we have the following problem:

$$\rho\ddot{\boldsymbol{\varphi}} = \boldsymbol{R}(\theta)\,\mathbf{div}\,\boldsymbol{\sigma}[\boldsymbol{\xi}] \qquad \text{in} \quad \Omega\times(0,T), \tag{3.14}$$

$$\boldsymbol{\xi} = \mathbf{0} \qquad \text{on} \quad \Gamma_D\times(0,T), \tag{3.15}$$

$$\boldsymbol{\sigma}[\boldsymbol{\xi}]\boldsymbol{n} = \mathbf{0} \qquad \text{on} \quad \Gamma_N\times(0,T). \tag{3.16}$$

Now, the deformation is decomposed by

$$\boldsymbol{\varphi} = \boldsymbol{R}(\theta)(\mathbf{id}+\boldsymbol{\xi}) \tag{3.17}$$

Then $\dot{\boldsymbol{\varphi}}$ and $\ddot{\boldsymbol{\varphi}}$ are calculated as following.

$$\begin{aligned}
\dot{\boldsymbol{\varphi}} &= \frac{\partial}{\partial t}\left\{\boldsymbol{R}(\theta)(\mathbf{id}+\boldsymbol{\xi})\right\}\\
&= \boldsymbol{R}(\theta)\boldsymbol{R}(\pi/2)\dot{\theta}(\mathbf{id}+\boldsymbol{\xi}) + \boldsymbol{R}(\theta)\dot{\boldsymbol{\xi}}\\
&= \boldsymbol{R}(\theta)\left\{\dot{\theta}\boldsymbol{R}(\pi/2)(\mathbf{id}+\boldsymbol{\xi}) + \dot{\boldsymbol{\xi}}\right\}\\
&=: \boldsymbol{R}(\theta)\boldsymbol{v}.
\end{aligned}$$

And we have

$$\begin{aligned}
\ddot{\boldsymbol{\varphi}} &= \mathbf{R}(\theta)\mathbf{R}(\pi/\mathbf{2})\dot{\theta}\left\{\dot{\theta}\mathbf{R}(\pi/\mathbf{2})(\mathbf{id}+\boldsymbol{\xi}) + \dot{\boldsymbol{\xi}}\right\} + \mathbf{R}(\theta)\left\{\ddot{\theta}\mathbf{R}(\pi/\mathbf{2})(\mathbf{id}+\boldsymbol{\xi}) + \dot{\theta}\mathbf{R}(\pi/\mathbf{2})\dot{\boldsymbol{\xi}} + \ddot{\boldsymbol{\xi}}\right\}\\
&= \mathbf{R}(\theta)\left\{\dot{\theta}^{\mathbf{2}}\mathbf{R}(\pi)(\mathbf{id}+\boldsymbol{\xi}) + \dot{\theta}\mathbf{R}(\pi/\mathbf{2})\dot{\boldsymbol{\xi}} + \ddot{\theta}\mathbf{R}(\pi/\mathbf{2})(\mathbf{id}+\boldsymbol{\xi}) + \dot{\theta}\mathbf{R}(\pi/\mathbf{2})\dot{\boldsymbol{\xi}} + \ddot{\boldsymbol{\xi}}\right\}\\
&= \mathbf{R}(\theta)\left\{-\dot{\theta}^{\mathbf{2}}(\mathbf{id}+\boldsymbol{\xi}) - \mathbf{2}\dot{\theta}\mathbf{R}(-\pi/\mathbf{2})\dot{\boldsymbol{\xi}} - \ddot{\theta}\mathbf{R}(-\pi/\mathbf{2})(\mathbf{id}+\boldsymbol{\xi}) + \ddot{\boldsymbol{\xi}}\right\},\\
&=: \boldsymbol{R}(\theta)\boldsymbol{a}.
\end{aligned}$$

where $\boldsymbol{v} := \dot{\theta}\boldsymbol{R}(\pi/2)(\mathbf{id}+\boldsymbol{\xi}) + \dot{\boldsymbol{\xi}}$, $\boldsymbol{a} := -\dot{\theta}^2(\mathbf{id}+\boldsymbol{\xi}) - 2\dot{\theta}\boldsymbol{R}(-\pi/2)\dot{\boldsymbol{\xi}} - \ddot{\theta}\boldsymbol{R}(-\pi/2)(\mathbf{id}+\boldsymbol{\xi}) + \ddot{\boldsymbol{\xi}}$.

Multiplying $\dot{\boldsymbol{\varphi}}$ in the both side of (3.14), and integrating over Ω, we obtain

$$\int_\Omega \rho\ddot{\boldsymbol{\varphi}}\cdot\dot{\boldsymbol{\varphi}}\,dx = \int_\Omega \mathbf{div}\,\boldsymbol{\sigma}[\boldsymbol{\xi}]\cdot\dot{\boldsymbol{\varphi}}\,dx. \tag{3.18}$$

Then we get

$$\begin{aligned}
\text{(l.h.s of (3.18))} &= \frac{1}{2}\frac{d}{dt}\int_\Omega \rho|\dot{\boldsymbol{\varphi}}|\,dx\\
&= \frac{1}{2}\frac{d}{dt}\int_\Omega \rho\boldsymbol{R}(\theta)\boldsymbol{v}\cdot\boldsymbol{R}(\theta)\boldsymbol{v}\,dx\\
&= \frac{1}{2}\frac{d}{dt}\int_\Omega \rho|\boldsymbol{v}|^2\,dx\\
&= \frac{1}{2}\frac{d}{dt}\int_\Omega \rho\left|\dot{\theta}\boldsymbol{R}(\pi/2)(\mathbf{id}+\boldsymbol{\xi}) + \dot{\boldsymbol{\xi}}\right|^2\,dx\\
&= \frac{1}{2}\frac{d}{dt}\int_\Omega \rho\left\{\left|\dot{\theta}^2\boldsymbol{R}(\pi/2)(\mathbf{id}+\boldsymbol{\xi})\right|^2 + 2\left[\dot{\theta}^2\boldsymbol{R}(\pi/2)(\mathbf{id}+\boldsymbol{\xi})\right]\cdot\dot{\boldsymbol{\xi}} + |\dot{\boldsymbol{\xi}}|^2\right\}\,dx\\
&= \frac{1}{2}\frac{d}{dt}\int_\Omega \rho\left\{\left[\dot{\theta}^2(\mathbf{id}+\boldsymbol{\xi}) + 2\dot{\theta}^2\boldsymbol{R}(-\pi/2)\dot{\boldsymbol{\varphi}}\right]\cdot(\mathbf{id}+\boldsymbol{\xi}) + |\dot{\boldsymbol{\xi}}|^2\right\}\,dx,
\end{aligned}$$

moreover

$$
\begin{aligned}
&\text{(r.h.s of (3.18))}\\
&= \int_\Omega \boldsymbol{R}(\theta)\,\mathbf{div}\,\boldsymbol{\sigma}[\boldsymbol{\xi}]\cdot\boldsymbol{R}(\theta)\boldsymbol{v}\,dx\\
&= \int_\Omega \mathbf{div}\,\boldsymbol{\sigma}[\boldsymbol{\xi}]\cdot\boldsymbol{v}\,dx\\
&= \int_\Omega \mathbf{div}\,\boldsymbol{\sigma}[\boldsymbol{\xi}]\cdot\left[\dot{\boldsymbol{\xi}}+\dot\theta\boldsymbol{R}(\pi/2)(\mathbf{id}+\boldsymbol{\xi})\right]\,dx\\
&= -\int_\Omega \boldsymbol{\sigma}[\boldsymbol{\xi}]:\boldsymbol{\epsilon}[\dot{\boldsymbol{\xi}}]\,dx-\int_\Omega \boldsymbol{\sigma}[\boldsymbol{\xi}]:\boldsymbol{\epsilon}\left[\dot\theta\boldsymbol{R}(\pi/2)(\mathbf{id}+\boldsymbol{\xi})\right]\,dx+\int_{\Gamma_D}\boldsymbol{\sigma}[\boldsymbol{\xi}]\boldsymbol{n}\cdot\left[\dot\theta\boldsymbol{R}(\pi/2)(\mathbf{id}+\boldsymbol{\xi})\right]\,ds\\
&= -\frac{1}{2}\frac{d}{dt}\int_\Omega \boldsymbol{\sigma}[\boldsymbol{\xi}]:\boldsymbol{\epsilon}[\boldsymbol{\xi}]\,dx-\int_\Omega \boldsymbol{\sigma}[\boldsymbol{\xi}]:\boldsymbol{\epsilon}\left[\dot\theta\boldsymbol{R}(\pi/2)(\mathbf{id}+\boldsymbol{\xi})\right]\,dx+\int_{\Gamma_D}\dot\theta|\mathbf{id}|\,(\boldsymbol{\sigma}[\boldsymbol{\xi}]\boldsymbol{n}\cdot\boldsymbol{t})\,ds,
\end{aligned}
$$

where $\boldsymbol{n}$ and $\boldsymbol{t}$ are unit outer normal vector and unit tangential vector of $\partial\Omega$, respectively.

We define the total energy by

$$
E[\boldsymbol{\xi}] := \frac{1}{2}\int_\Omega \rho\left\{\left[\dot\theta^2(\mathbf{id}+\boldsymbol{\xi})+2\dot\theta^2\boldsymbol{R}(-\pi/2)\dot{\boldsymbol{\varphi}}\right]\cdot(\mathbf{id}+\boldsymbol{\xi})+|\dot{\boldsymbol{\xi}}|^2\right\}\,dx+\frac{1}{2}\int_\Omega\boldsymbol{\sigma}[\boldsymbol{\xi}]:\boldsymbol{\epsilon}[\boldsymbol{\xi}]\,dx. \tag{3.19}
$$

Now we get the equations

$$
\frac{d}{dt}E[\boldsymbol{\xi}](t) = -\int_\Omega \boldsymbol{\sigma}[\boldsymbol{\xi}]:\boldsymbol{\epsilon}\left[\dot\theta\boldsymbol{R}(\pi/2)(\mathbf{id}+\boldsymbol{\xi})\right]\,dx+\int_{\Gamma_D}\dot\theta|\mathbf{id}|\,(\boldsymbol{\sigma}[\boldsymbol{\xi}]\boldsymbol{n}\cdot\boldsymbol{t})\,ds \tag{3.20}
$$

for all $t>0$.

3.4 Boundary conditions

We subdivide the boundary $\partial\Omega$ into Γ_D and Γ_C (see Figure 3.2), where

$$
\Gamma_D\cup\Gamma_C=\partial\Omega,\quad \Gamma_D\cap\Gamma_C=\emptyset,\quad \Gamma_D\neq\emptyset. \tag{3.21}
$$

On the boundary Γ_D we model the forced rotation of Ω by imposing the Dirichlet boundary condition

$$
\boldsymbol{\varphi}(\boldsymbol{x})=\boldsymbol{R}\boldsymbol{x}\quad \text{for } \boldsymbol{x}\in\Gamma_D, \tag{3.22}
$$

which is equivalent to

$$
\boldsymbol{\xi}=\mathbf{0}\quad \text{on } \Gamma_D. \tag{3.23}
$$

We describe the height of the obstacle by a smooth function $g:[0,T)\to\mathbb{R}$. The condition that the deformed configuration remains above the obstacle is given by

$$
\varphi_2(\boldsymbol{x})=(\boldsymbol{x}+\boldsymbol{\xi}(\boldsymbol{x}))\cdot\left(\boldsymbol{R}^T\boldsymbol{e}_2\right)\geq g\quad \text{for all } \boldsymbol{x}\in\Gamma_C, \tag{3.24}
$$

where $\boldsymbol{e}_i\in\mathbb{R}^2$ are the unit vectors of the canonical basis in the Lagrangian frame. We call

$$
\{\boldsymbol{\varphi}(\boldsymbol{x});\boldsymbol{x}\in\Gamma_C,\ \varphi_2(\boldsymbol{x})=g\},
$$

the contact zone, and note that it is an unknown subset of Γ_C.

Using the contact zone, we describe the boundary conditions on Γ_C. Outside of the contact zone, we impose homogeneous Neumann boundary conditions (i.e., zero traction). At the contact zone, we impose zero traction in tangential direction (i.e., no friction force between the elastic body and the obstacle), and require the normal force of the obstacle on the elastic body to be non-negative. This leads to the following boundary conditions on Γ_C:

$$\begin{aligned} (\mathbf{id} + \boldsymbol{\xi}) \cdot \left(\boldsymbol{R}^T \boldsymbol{e}_2\right) &\geq g \\ (\boldsymbol{\sigma}[\boldsymbol{\xi}]\boldsymbol{n}) \cdot \left(\boldsymbol{R}^T \boldsymbol{e}_1\right) &= 0 \\ (\boldsymbol{\sigma}[\boldsymbol{\xi}]\boldsymbol{n}) \cdot \left(\boldsymbol{R}^T \boldsymbol{e}_2\right) &\geq 0 \\ \left((\mathbf{id} + \boldsymbol{\xi}) \cdot \left(\boldsymbol{R}^T \boldsymbol{e}_2\right) - g\right) (\boldsymbol{\sigma}[\boldsymbol{\xi}]\boldsymbol{n}) \cdot \left(\boldsymbol{R}^T \boldsymbol{e}_2\right) &= 0 \end{aligned} \qquad \text{on } \Gamma_C, \tag{3.25}$$

where $\boldsymbol{n}$ is the unit outward normal vector to Γ_C.

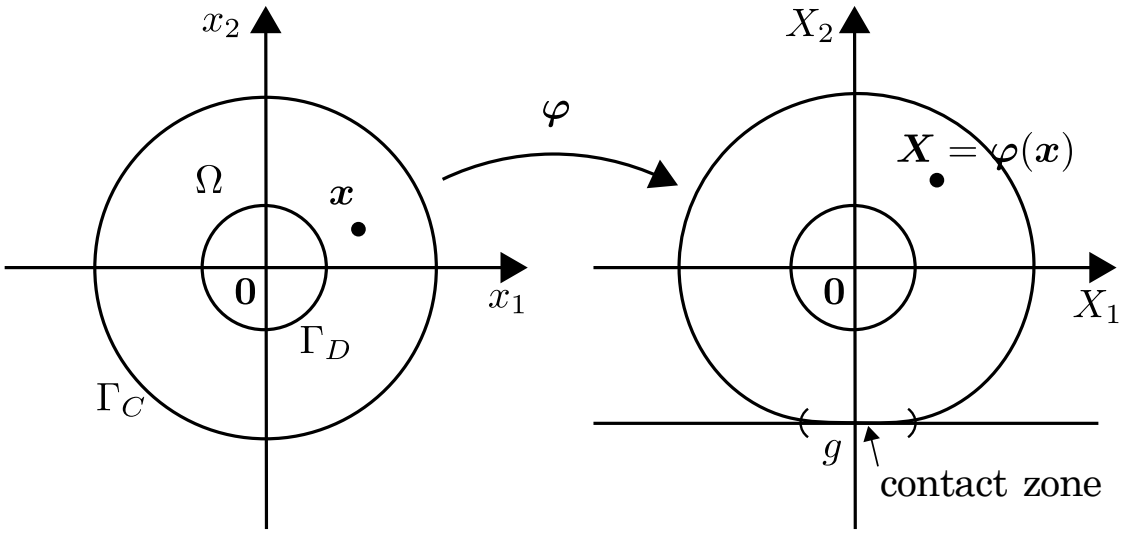

Figure 3.2: Sketch of the boundary components Γ_D, Γ_C and the contact zone.

3.5 Full model

Summarizing the equations above, and adding initial conditions, we obtain the complete system

$$
\text{(P)}\quad \begin{cases}
\rho\ddot{\boldsymbol{\xi}} - \mathbf{div}\,\boldsymbol{\sigma}[\boldsymbol{\xi}] = \rho\boldsymbol{f}(\cdot,\cdot,\boldsymbol{\xi},\dot{\boldsymbol{\xi}}) \quad \text{in} \quad \Omega\times(0,T),\\
\boldsymbol{\xi} = \mathbf{0} \quad \text{on} \quad \Gamma_D\times[0,T),\\
(\mathbf{id}+\boldsymbol{\xi})\cdot\left(\boldsymbol{R}^T(\theta)\boldsymbol{e}_2\right) \geq g \quad \text{on} \quad \Gamma_C\times[0,T),\\
(\boldsymbol{\sigma}[\boldsymbol{\xi}]\boldsymbol{n})\cdot\left(\boldsymbol{R}^T(\theta)\boldsymbol{e}_1\right) = 0 \quad \text{on} \quad \Gamma_C\times[0,T),\\
(\boldsymbol{\sigma}[\boldsymbol{\xi}]\boldsymbol{n})\cdot\left(\boldsymbol{R}^T(\theta)\boldsymbol{e}_2\right) \geq 0 \quad \text{on} \quad \Gamma_C\times[0,T),\\
\left((\mathbf{id}+\boldsymbol{\xi})\cdot\left(\boldsymbol{R}^T(\theta)\boldsymbol{e}_2\right)-g\right)(\boldsymbol{\sigma}[\boldsymbol{\xi}]\boldsymbol{n})\cdot\left(\boldsymbol{R}^T(\theta)\boldsymbol{e}_2\right) = 0 \quad \text{on} \quad \Gamma_C\times[0,T),\\
\boldsymbol{\xi}(\cdot,0) = \boldsymbol{\xi}^0 \quad \text{in} \quad \Omega,\\
\dot{\boldsymbol{\xi}}(\cdot,0) = \boldsymbol{\eta}^0 \quad \text{in} \quad \Omega.
\end{cases}
$$

where $\theta, g : [0,T) \to \mathbb{R}$ and $\boldsymbol{\xi}^0, \boldsymbol{\eta}^0$ are given functions, and $\boldsymbol{f}$ is defined in (3.13). (P) describes the complete set of equations of motion for $\boldsymbol{\xi}$ which we solve numerically in the remainder of this paper.

Chapter 4

Numerical method

In this section, we describe and apply the discrete Morse flow (DMF) to discretize (P). The idea is to discretize (P) in time by using the implicit Crank-Nicolson scheme (§4.1 This results in a scheme where at each time step an elliptic obstacle problem needs to be solved. In §4.2 we derive a variational structure of this elliptic obstacle problem. In §4.4 we adjust the nonlinear conjugate gradient method to find a minimizer of the related minimization problem.

4.1 Time-discretized problem

For the discretization in time, let $T > 0$ be the end time, $M \in \mathbb{N}$ be the number of time steps, and $\Delta t := T/M$ the time step size. For each time step $k = 0, 1, \cdots, M$, we set

$$\theta^k := \theta(k\Delta t), \quad g^k := g(k\Delta t),$$

and denote by $\boldsymbol{\xi}^k : \Omega \to \mathbb{R}^2$ the time-discretized approximation of the solution $\boldsymbol{\xi}$ of (P) at time $k\Delta t$. For convenience, we set $\boldsymbol{\xi}^k|_{k=-1} := \boldsymbol{\xi}^0 - \Delta t \boldsymbol{\eta}^0$.

Using the Crank-Nicolson scheme, we discretize the elastodynamics equation in time as

$$\rho \frac{\boldsymbol{\xi}^k - 2\boldsymbol{\xi}^{k-1} + \boldsymbol{\xi}^{k-2}}{(\Delta t)^2} = \mathbf{div}\, \boldsymbol{\sigma}\left[\frac{\boldsymbol{\xi}^k + \boldsymbol{\xi}^{k-2}}{2}\right] + \rho \boldsymbol{f}^{k-1} \quad \text{in } \Omega, \tag{4.1}$$

where we define

$$\boldsymbol{f}^{k-1}(\boldsymbol{x}) := \boldsymbol{f}((k-1)\Delta t, \boldsymbol{x}, \boldsymbol{\xi}^{k-1}, (\boldsymbol{\xi}^{k-1} - \boldsymbol{\xi}^{k-2})/\Delta t). \tag{4.2}$$

Using the definition of $\boldsymbol{f}$, (4.2) reads

$$\boldsymbol{f}^{k-1}(\boldsymbol{x}) = \ddot{\theta}^{k-1}\boldsymbol{R}(-\pi/2)(\boldsymbol{x} + \boldsymbol{\xi}^{k-1}) + (\dot{\theta}^{k-1})^2(\boldsymbol{x} + \boldsymbol{\xi}^{k-1}) + 2\dot{\theta}^{k-1}\boldsymbol{R}(-\pi/2)\frac{\boldsymbol{\xi}^{k-1} - \boldsymbol{\xi}^{k-2}}{\Delta t}. \tag{4.3}$$

The advantage of the Crank-Nicolson scheme in contrast to the purely implicit scheme used in previous works [28] is that it conserves the time-discrete energy in the case when $\theta \equiv 0$ with homogeneous Dirichlet boundary conditions:

Theorem 1. *(K.Švadlenka) If $\theta \equiv 0$, $\boldsymbol{\xi}^k = \mathbf{0}$ on $\partial\Omega$ for $k = 0, 1, \cdots, M$, and $\boldsymbol{\xi}^k$ satisfies (4.1) for $k = 1, 2 \cdots, M$, then the time-discrete energy*

$$E^k := \frac{1}{2}\int_\Omega \frac{|\boldsymbol{\xi}^k - \boldsymbol{\xi}^{k-1}|^2}{(\Delta t)^2}\,dx + \frac{1}{2}\int_\Omega \frac{\boldsymbol{\sigma}[\boldsymbol{\xi}^k] : \boldsymbol{\epsilon}[\boldsymbol{\xi}^k] + \boldsymbol{\sigma}[\boldsymbol{\xi}^{k-1}] : \boldsymbol{\epsilon}[\boldsymbol{\xi}^{k-1}]}{2}\,dx \quad \text{for } k = 1, 2, \cdots, M \tag{4.4}$$

does not depend on k. Here, $\boldsymbol{\sigma} : \boldsymbol{\epsilon} := \sigma_{ij}\epsilon_{ij}$.

Proof. Multiplying both sides of (4.1) by $\boldsymbol{\xi}^k - \boldsymbol{\xi}^{k-2}$, integrating over Ω and integrating by parts, we get

$$\int_\Omega \frac{\boldsymbol{\xi}^k - 2\boldsymbol{\xi}^{k-1} + \boldsymbol{\xi}^{k-2}}{(\Delta t)^2} \cdot (\boldsymbol{\xi}^k - \boldsymbol{\xi}^{k-2})\,dx = \int_\Omega \mathbf{div}\,\boldsymbol{\sigma}\left[\frac{\boldsymbol{\xi}^k + \boldsymbol{\xi}^{k-2}}{2}\right] \cdot (\boldsymbol{\xi}^k - \boldsymbol{\xi}^{k-2})\,dx,$$

moreover we obtain

$$\int_\Omega \frac{|\boldsymbol{\xi}^k|^2 - |\boldsymbol{\xi}^{k-2}|^2 - 2\boldsymbol{\xi}^k \cdot \boldsymbol{\xi}^{k-1} + 2\boldsymbol{\xi}^{k-1} \cdot \boldsymbol{\xi}^{k-2}}{(\Delta t)^2}\,dx = -\int_\Omega \frac{1}{2}\left(\boldsymbol{\sigma}[\boldsymbol{\xi}^k] : \boldsymbol{\epsilon}[\boldsymbol{\xi}^k] - \boldsymbol{\sigma}[\boldsymbol{\xi}^{k-2}] : \boldsymbol{\epsilon}[\boldsymbol{\xi}^{k-2}]\right)\,dx.$$

Summing over $k = 2$ to K, we obtain

$$E^1 = E^K, \tag{4.5}$$

for $K = 2, 3, \cdots, M$. □

The Crank-Nicolson discretization above yields the following time-discretized scheme for (P). The choice of $(\boldsymbol{\xi}^k + \boldsymbol{\xi}^{k-2})/2$ in the boundary conditions is motivated by the variational formula that we explain in detail in the next §4.2. Let $\boldsymbol{\xi}^0, \boldsymbol{\eta}^0 \in W^{1,2}(\Omega; \mathbb{R}^2)$ be given, and set $\boldsymbol{\xi}^k|_{k=-1} := \boldsymbol{\xi}^0 - \Delta t\boldsymbol{\eta}^0$. For $k = 1, 2, \cdots, M$, find $\boldsymbol{\xi}^k : \Omega \to \mathbb{R}^2$ such that the following equations are satisfied:

$$(\mathrm{P}_k)\begin{cases} \rho\dfrac{\boldsymbol{\xi}^k - 2\boldsymbol{\xi}^{k-1} + \boldsymbol{\xi}^{k-2}}{(\Delta t)^2} - \mathbf{div}\,\boldsymbol{\sigma}\left[\dfrac{\boldsymbol{\xi}^k + \boldsymbol{\xi}^{k-2}}{2}\right] = \rho\boldsymbol{f}^{k-1} & \text{in} \quad \Omega, \\ \boldsymbol{\xi}^k = \mathbf{0} & \text{on} \quad \Gamma_D, \\ (\mathbf{id} + \boldsymbol{\xi}^k) \cdot \left(\boldsymbol{R}^T(\theta^k)\boldsymbol{e}_2\right) \geq g^k & \text{on} \quad \Gamma_C, \\ \left(\boldsymbol{\sigma}\left[\dfrac{\boldsymbol{\xi}^k + \boldsymbol{\xi}^{k-2}}{2}\right]\boldsymbol{n}\right) \cdot \left(\boldsymbol{R}^T(\theta^k)\boldsymbol{e}_1\right) = 0 & \text{on} \quad \Gamma_C, \\ \left(\boldsymbol{\sigma}\left[\dfrac{\boldsymbol{\xi}^k + \boldsymbol{\xi}^{k-2}}{2}\right]\boldsymbol{n}\right) \cdot \left(\boldsymbol{R}^T(\theta^k)\boldsymbol{e}_2\right) \geq 0 & \text{on} \quad \Gamma_C, \\ \left((\mathbf{id} + \boldsymbol{\xi}^k) \cdot \left(\boldsymbol{R}^T(\theta^k)\boldsymbol{e}_2\right) - g^k\right)\left(\boldsymbol{\sigma}\left[\dfrac{\boldsymbol{\xi}^k + \boldsymbol{\xi}^{k-2}}{2}\right]\boldsymbol{n}\right) \cdot \left(\boldsymbol{R}^T(\theta^k)\boldsymbol{e}_2\right) = 0 & \text{on} \quad \Gamma_C. \end{cases}$$

The convergence of the proposed numerical scheme based on the Crank-Nicolson time discretization is the subject of future work. However, the purely implicit time discretization was used previously to show the existence of a weak solution for a system of hyperbolic equations without a constraint in [30], and with constraint for a single equation in [28].

4.2 Variational structure of the time-discretized problem

For any $k = 1, 2, \cdots, M$, problem (P_k) is an elliptic problem with an obstacle. It is the Euler-Lagrange equation for the minimizer of the functional

$$\mathcal{J}^k(\boldsymbol{\xi}) := \rho \int_\Omega \frac{|\boldsymbol{\xi} - 2\boldsymbol{\xi}^{k-1} + \boldsymbol{\xi}^{k-2}|^2}{2(\Delta t)^2}\, dx + \frac{1}{2}\int_\Omega \left(\frac{1}{2}\boldsymbol{\sigma}[\boldsymbol{\xi}] + \boldsymbol{\sigma}[\boldsymbol{\xi}^{k-2}]\right) : \boldsymbol{\epsilon}[\boldsymbol{\xi}]\, dx - \rho\int_\Omega \boldsymbol{f}^{k-1}\cdot\boldsymbol{\xi}\, dx, \tag{4.6}$$

over to the admissible set

$$\mathcal{K}^k := \left\{\boldsymbol{\xi} \in W^{1,2}(\Omega;\mathbb{R}^2);\ \boldsymbol{\xi} = \mathbf{0} \text{ a.e. on } \Gamma_D,\ (\mathbf{id} + \boldsymbol{\xi})\cdot\left(\boldsymbol{R}^T(\theta^k)\boldsymbol{e}_2\right) \geq g^k \text{ a.e. on } \Gamma_C\right\}. \tag{4.7}$$

Indeed, by calculating the first variation of $\mathcal{J}^k$ over $\mathcal{K}^k$ we obtain that any minimizer $\boldsymbol{\xi}^k$ satisfies (P_k). The existence of a unique minimizer follows from the facts that $\mathcal{J}^k$ is weakly lower semi–continuous on $W^{1,2}(\Omega;\mathbb{R}^2)$, is bounded from below, has bounded sublevel sets, and that $\mathcal{K}^k$ is convex and closed in $W^{1,2}(\Omega;\mathbb{R}^2)$. Let us check that the sufficiently smooth minimizer $\boldsymbol{\xi}^k$ satisfies (P_k) by the analogy of [9]. The minimizer $\boldsymbol{\xi}^k$ satisfies the inequality

$$\mathcal{J}^k(\boldsymbol{\eta}) \geq \mathcal{J}^k(\boldsymbol{\xi}^k) \qquad \text{for all } \boldsymbol{\eta} \in \mathcal{K}^k.$$

Taking any $\boldsymbol{\psi} \in C^\infty(\overline{\Omega};\mathbb{R}^2)$ such that $\boldsymbol{\eta} = \boldsymbol{\xi}^k + s\boldsymbol{\psi} \in \mathcal{K}^k$ for small $s \geq 0$, expanding $\mathcal{J}^k(\boldsymbol{\xi}^k + s\boldsymbol{\psi})$ in terms of s, we deduce that the first-order term in s must be non-negative, that is,

$$\rho\int_\Omega \frac{(\boldsymbol{\xi}^k - 2\boldsymbol{\xi}^{k-1} + \boldsymbol{\xi}^{k-2})\cdot\boldsymbol{\psi}}{(\Delta t)^2}\, dx + \int_\Omega \boldsymbol{\sigma}\left[\frac{\boldsymbol{\xi}^k + \boldsymbol{\xi}^{k-2}}{2}\right] : \boldsymbol{\epsilon}[\boldsymbol{\psi}]\, dx - \rho\int_\Omega \boldsymbol{f}^{k-1}\cdot\boldsymbol{\psi}\, dx \geq 0. \tag{4.8}$$

Integrating by parts, we have

$$\begin{aligned} 0 \leq \int_\Omega \left(\rho\frac{(\boldsymbol{\xi}^k - 2\boldsymbol{\xi}^{k-1} + \boldsymbol{\xi}^{k-2})}{(\Delta t)^2} - \mathbf{div}\,\boldsymbol{\sigma}\left[\frac{\boldsymbol{\xi}^k + \boldsymbol{\xi}^{k-2}}{2}\right] - \rho\boldsymbol{f}^{k-1}\right)\cdot\boldsymbol{\psi}\, dx \\ + \int_{\Gamma_C}\left(\boldsymbol{\sigma}\left[\frac{\boldsymbol{\xi}^k + \boldsymbol{\xi}^{k-2}}{2}\right]\boldsymbol{n}\right)\cdot\boldsymbol{\psi}\, ds. \end{aligned} \tag{4.9}$$

Choosing $\boldsymbol{\psi} \in C_0^\infty(\Omega;\mathbb{R}^2)$, (4.9) implies the first equation in (P_k). Thus for $\boldsymbol{\psi} \in C^\infty(\overline{\Omega};\mathbb{R}^2)$, we deduce from (4.9)

$$\begin{aligned} 0 &\leq \int_{\Gamma_C}\left(\boldsymbol{\sigma}\left[\frac{\boldsymbol{\xi}^k + \boldsymbol{\xi}^{k-2}}{2}\right]\boldsymbol{n}\right)\cdot\boldsymbol{\psi}\, ds \\ &= \int_{\Gamma_C}\sum_{i=1}^{2}\left\{\left(\boldsymbol{\sigma}\left[\frac{\boldsymbol{\xi}^k + \boldsymbol{\xi}^{k-2}}{2}\right]\boldsymbol{n}\right)\cdot\left(\boldsymbol{R}^T(\theta^k)\boldsymbol{e}_i\right)\right\}\left\{\boldsymbol{\psi}\cdot\left(\boldsymbol{R}^T(\theta^k)\boldsymbol{e}_i\right)\right\} ds. \end{aligned} \tag{4.10}$$

If we choose $\boldsymbol{\psi}$ such that

$$\boldsymbol{\psi}\cdot\left(\boldsymbol{R}^T(\theta^k)\boldsymbol{e}_2\right) = 0 \quad \text{ on } \Gamma_C,$$

we deduce the fourth equation of (P_k). And if we choose a function $\boldsymbol{\psi}$ such that

$$\boldsymbol{\psi} \cdot \left(\boldsymbol{R}^T(\theta^k)\boldsymbol{e}_2\right) \geq 0 \quad \text{on } \Gamma_C,$$

then $\boldsymbol{\eta} = \boldsymbol{\xi}^k + s\boldsymbol{\psi} \in \mathcal{K}^k$ for small $s \geq 0$ and (4.10) yields the fifth equation of (P_k). Finally, suppose that $(\mathbf{id} + \boldsymbol{\xi}^k) \cdot \left(\boldsymbol{R}^T(\theta^k)\boldsymbol{e}_2\right) - g^k > 0$ at a point $\boldsymbol{x} \in \Gamma_C$. Then there exists $\boldsymbol{\psi} \in C^\infty(\overline{\Omega}; \mathbb{R}^2)$ such that

$$\boldsymbol{\psi} \cdot \left(\boldsymbol{R}^T(\theta^k)\boldsymbol{e}_2\right)(\boldsymbol{x}) < 0 \quad \text{and} \quad (\mathbf{id} + \boldsymbol{\xi}^k + s\boldsymbol{\psi}) \cdot \left(\boldsymbol{R}^T(\theta^k)\boldsymbol{e}_2\right) - g^k \geq 0 \quad \text{on } \Gamma_C \text{ for small } s \geq 0.$$

Condition (4.10) together with the fifth equation implies

$$\left(\boldsymbol{\sigma}\left[\frac{\boldsymbol{\xi}^k(\boldsymbol{x}) + \boldsymbol{\xi}^{k-2}(\boldsymbol{x})}{2}\right]\boldsymbol{n}(\boldsymbol{x})\right) \cdot \left(\boldsymbol{R}^T(\theta^k)\boldsymbol{e}_2\right) = 0,$$

and therefore the last equation in (P_k) holds.

4.3 Existence of the minimizer

In this section, we discuss the existence of the minimizer of $\mathcal{J}^k$ on $\mathcal{K}^k$ defined by (4.6) and (4.7). We apply the general theory (see [5]).

Theorem 2. *Suppose V, $\mathcal{K}$ and $\mathcal{J} : \mathcal{K} \to \mathbb{R}$ satisfy the following hypothesis:*

($H1$) *V is reflexive Banach space,*

($H2$) *$\mathcal{K}$ is weakly closed,*

($H3$) *$\mathcal{K}$ is bounded and*

($H4$) *$\mathcal{J} : \mathcal{K} \subset V \to \mathbb{R}$ is weakly lower semi–continuous.*

Then $\mathcal{J}$ has a global minimum in $\mathcal{K}$.

Proof. We take a minimizing sequence $\{v_n\}_{n\in\mathbb{N}} \subset \mathcal{K}$:

$$\mathcal{J}(v_n) \searrow \inf_{v\in\mathcal{K}} \mathcal{J}(v)$$

Since $\mathcal{K}$ is bounded, $\{v_n\}_{n\in\mathbb{N}}$ is also bounded. V is reflexive Banach space, therefore there exists a weakly converging subsequence $\{v_{n_j}\}_{j\in\mathbb{N}}$ and $w \in V$ such that

$$v_{n_j} \rightharpoonup w \quad \text{in } V \quad \text{as } j \to \infty.$$

Since $\mathcal{K}$ is weakly closed, w belongs to $\mathcal{K}$. Using the weakly lower semi–continuity of $\mathcal{J}$, we have

$$\mathcal{J}(w) \leq \liminf_{j\to\infty} \mathcal{J}(v_{n_j}) = \inf_{v\in\mathcal{K}} \mathcal{J}(v).$$

Therefore w is the minimizer of $\mathcal{J}$ in $\mathcal{K}$. □

Theorem 3. *If V, $\mathcal{K}$ and $\mathcal{J} : \mathcal{K} \to \mathbb{R}$ satisfy the hypothesis $(H1)$, $(H2)$, $(H4)$ and $\mathcal{J}$ satisfies*

$$(H3)' \qquad \lim_{\|v\|_V \to \infty} \mathcal{J}(v) = \infty,$$

then $\mathcal{J}$ has a global minimum in $\mathcal{K}$.

Proof. Let $v_0 \in \mathcal{K}$ be arbitrary fixed, and define a admissible set

$$\mathcal{K}_0 := \{v \in \mathcal{K}; \mathcal{J}(v) \leq \mathcal{J}(v_0)\}$$

If there exists a minimizer of $\mathcal{J}$ in $\mathcal{K}_0$, the minimizer is also a minimizer of $\mathcal{J}$ in $\mathcal{K}$. Indeed, let w be a minimizer of $\mathcal{J}$ in $\mathcal{K}_0$.

$$\mathcal{J}(w) \leq \inf_{v \in \mathcal{K}_0} \mathcal{J}(v) = \inf_{v \in \mathcal{K}} \mathcal{J}(v),$$

hence w is a minimizer of $\mathcal{J}$ in $\mathcal{K}$. Our goal is that we show the existence of a minimizer of $\mathcal{J}$ in $\mathcal{K}_0$. As the goal, we show $\mathcal{K}_0$ is bounded and weakly closed in V. Suppose $\mathcal{K}_0$ is not bounded then there exists $\{v_n\}_{n \in \mathbb{N}} \subset \mathcal{K}_0$ such that

$$\|v_n\|_V \to \infty \quad \text{as } n \to \infty.$$

Then by $(H3)'$, $\mathcal{J}(v_n) \to \infty$ as $n \to \infty$ which is contradiction for the definition of $\mathcal{K}_0$. Hence $\mathcal{K}_0$ is bounded. As last step, we show that $\mathcal{K}_0$ is weakly closed. Let $\{v_n\} \subset \mathcal{K}_0$; $v_n \rightharpoonup w$ in V as $n \to \infty$. Since $\mathcal{J}$ is weakly lower semi–continuous, we obtain

$$\mathcal{J}(w) \leq \liminf_{n \to \infty} \mathcal{J}(v_n) \leq \mathcal{J}(v_0).$$

Hence $w \in \mathcal{K}_0$. Now $\mathcal{K}_0$ and $\mathcal{J}$ satisfy all the hypothesis of Theorem 2. □

Theorem 4. *There exists a minimizer of $\mathcal{J}^k$ on $\mathcal{K}^k$ defined by* (4.6) *and* (4.7).

Proof. $W^{1,2}(\Omega; \mathbb{R}^2)$ is reflexive Banach space. We claim that $\mathcal{K}^k$ is closed and convex set. To show that $\mathcal{K}^k$ is closed, let $\{\boldsymbol{\xi}_n\} \subset \mathcal{K}^k$; $\boldsymbol{\xi}_n \to \boldsymbol{\xi}$ in $W^{1,2}(\Omega; \mathbb{R}^2)$ as $n \to \infty$.

$$\begin{aligned} \gamma((\boldsymbol{\xi}_n)_i) &= 0 && \text{a.e. on } \Gamma_D, \\ \Big(\mathbf{id} + \big(\gamma((\boldsymbol{\xi}_n)_i)\big)\Big) \cdot \Big(\boldsymbol{R}^T(\theta^k)\boldsymbol{e}_2\Big) &\geq g^k && \text{a.e. on } \Gamma_N. \end{aligned}$$

Since the trace operator $\gamma : W^{1,2}(\Omega) \to L^2(\partial\Omega)$ is bounded linear operator, we have

$$\begin{aligned} \gamma((\boldsymbol{\xi})_i) &= 0 && \text{a.e. on } \Gamma_D, \\ \Big(\mathbf{id} + \big(\gamma((\boldsymbol{\xi})_i)\big)\Big) \cdot \Big(\boldsymbol{R}^T(\theta^k)\boldsymbol{e}_2\Big) &\geq g^k && \text{a.e. on } \Gamma_N. \end{aligned}$$

Hence $\mathcal{K}^k$ is closed. To show that $\mathcal{K}^k$ is convex, let $\boldsymbol{\xi}, \boldsymbol{\eta} \in \mathcal{K}^k$ and $\alpha \in (0, 1)$.

$$\begin{aligned} &\Big(\mathbf{id} + \big(\alpha\boldsymbol{\xi} + (1-\alpha)\boldsymbol{\eta}\big)\Big) \cdot \Big(\boldsymbol{R}^T(\theta^k)\boldsymbol{e}_2\Big) \\ &= \Big(\alpha\big(\mathbf{id} + \boldsymbol{\xi}\big) + (1-\alpha)\big(\mathbf{id} + \boldsymbol{\eta}\big)\Big) \cdot \Big(\boldsymbol{R}^T(\theta^k)\boldsymbol{e}_2\Big) \\ &= \alpha\big(\mathbf{id} + \boldsymbol{\xi}\big) \cdot \Big(\boldsymbol{R}^T(\theta^k)\boldsymbol{e}_2\Big) + (1-\alpha)\big(\mathbf{id} + \boldsymbol{\eta}\big) \cdot \Big(\boldsymbol{R}^T(\theta^k)\boldsymbol{e}_2\Big) \\ &\geq \alpha g^k + (1-\alpha) g^k = g^k, \end{aligned}$$

for almost everywhere on Γ_C. Hence $\mathcal{K}^k$ is convex. We apply the theorem by Mazur's that $\mathcal{K}^k$ is weakly closed. As next step, we claim that $\mathcal{J}^k$ is weakly lower semi–continuous in $W^{1,2}(\Omega;\mathbb{R}^2)$ and satisfies

$$\lim_{\|\boldsymbol{\xi}\|_{W^{1,2}(\Omega;\mathbb{R}^2)}\to\infty} \mathcal{J}^k(\boldsymbol{\xi}) = \infty.$$

To prove that $\mathcal{J}^k$ satisfies $(H3)'$, we estimate $\mathcal{J}^k$ from the below.

$$\begin{aligned}
&\mathcal{J}^k(\boldsymbol{\xi}) \\
&\geq \frac{\rho}{2(\Delta t)^2}\left(\left\|\boldsymbol{\xi}+\boldsymbol{\xi}^{k-2}\right\|_{L^2(\Omega;\mathbb{R}^2)} - 2\left\|\boldsymbol{\xi}^{k-1}\right\|_{L^2(\Omega;\mathbb{R}^2)}\right)^2 + \frac{1}{4}\int_\Omega \boldsymbol{\sigma}[\boldsymbol{\xi}+\boldsymbol{\xi}^{k-2}] : \boldsymbol{\epsilon}[\boldsymbol{\xi}+\boldsymbol{\xi}^{k-2}]\,dx \\
&\quad - \frac{1}{4}\int_\Omega \boldsymbol{\sigma}[\boldsymbol{\xi}^{k-2}] : \boldsymbol{\epsilon}[\boldsymbol{\xi}^{k-2}]\,dx - \rho\left\|\boldsymbol{f}^{k-1}\right\|_{L^2(\Omega;\mathbb{R}^2)}\|\boldsymbol{\xi}\|_{L^2(\Omega;\mathbb{R}^2)} \\
&\geq \frac{\rho}{2(\Delta t)^2}\left(\left\|\boldsymbol{\xi}+\boldsymbol{\xi}^{k-2}\right\|^2_{L^2(\Omega;\mathbb{R}^2)} - 4\left\|\boldsymbol{\xi}^{k-1}\right\|_{L^2(\Omega;\mathbb{R}^2)}\left\|\boldsymbol{\xi}+\boldsymbol{\xi}^{k-2}\right\|_{W^{1,2}(\Omega;\mathbb{R}^2)}\right) \\
&\quad + \frac{\mu}{2}\left\|\nabla(\boldsymbol{\xi}+\boldsymbol{\xi}^{k-2})\right\|^2_{L^2(\Omega;\mathbb{R}^2)} - \frac{1}{4}\int_\Omega \boldsymbol{\sigma}[\boldsymbol{\xi}^{k-2}] : \boldsymbol{\epsilon}[\boldsymbol{\xi}^{k-2}]\,dx - \rho\left\|\boldsymbol{f}^{k-1}\right\|_{L^2(\Omega;\mathbb{R}^2)}\|\boldsymbol{\xi}\|_{W^{1,2}(\Omega;\mathbb{R}^2)} \\
&\geq C_m\left\|\boldsymbol{\xi}+\boldsymbol{\xi}^{k-2}\right\|^2_{W^{1,2}(\Omega;\mathbb{R}^2)} - \widetilde{C}_M\|\boldsymbol{\xi}\|_{W^{1,2}(\Omega;\mathbb{R}^2)} - C_0 \\
&\geq C_m\|\boldsymbol{\xi}\|^2_{W^{1,2}(\Omega;\mathbb{R}^2)} - C_M\|\boldsymbol{\xi}\|_{W^{1,2}(\Omega;\mathbb{R}^2)} - C_0,
\end{aligned}$$

where we set

$$\begin{aligned}
C_m &:= \min\left\{\frac{\rho}{2(\Delta t)^2}, \frac{\mu}{2}\right\}, \\
\widetilde{C}_M &:= \frac{2\rho}{(\Delta t)^2}\left\|\boldsymbol{\xi}^{k-1}\right\|_{L^2(\Omega;\mathbb{R}^2)} + \rho\left\|\boldsymbol{f}^{k-1}\right\|_{L^2(\Omega;\mathbb{R}^2)}, \\
C_M &:= 2C_m\left\|\boldsymbol{\xi}^{k-2}\right\|_{W^{1,2}(\Omega;\mathbb{R}^2)} + \frac{2\rho}{(\Delta t)^2}\left\|\boldsymbol{\xi}^{k-1}\right\|_{L^2(\Omega;\mathbb{R}^2)} + \rho\left\|\boldsymbol{f}^{k-1}\right\|_{L^2(\Omega;\mathbb{R}^2)}, \\
C_0 &:= -\frac{2\rho}{(\Delta t)^2}\left\|\boldsymbol{\xi}^{k-1}\right\|_{L^2(\Omega;\mathbb{R}^2)}\left\|\boldsymbol{\xi}^{k-2}\right\|_{W^{1,2}(\Omega;\mathbb{R}^2)} - \frac{1}{4}\int_\Omega \boldsymbol{\sigma}[\boldsymbol{\xi}^{k-2}] : \boldsymbol{\epsilon}[\boldsymbol{\xi}^{k-2}]\,dx.
\end{aligned}$$

Hence $(H3)'$ holds. As the last step, we show the weakly lower semi–continuous of $\mathcal{J}^k$ in $W^{1,2}(\Omega;\mathbb{R}^2)$. We expand $\mathcal{J}^k$ as following.

$$\begin{aligned}
\mathcal{J}^k(\boldsymbol{\xi}) = \frac{\rho}{2(\Delta t)^2}&\left(\int_\Omega |\boldsymbol{\xi}|^2\,dx - 2\int_\Omega \boldsymbol{\xi}\cdot(2\boldsymbol{\xi}^{k-1}-\boldsymbol{\xi}^{k-2})\,dx + \int_\Omega |2\boldsymbol{\xi}^{k-1}-\boldsymbol{\xi}^{k-2}|^2\,dx\right) \\
&+ \frac{1}{4}\int_\Omega \boldsymbol{\sigma}[\boldsymbol{\xi}] : \boldsymbol{\epsilon}[\boldsymbol{\xi}]\,dx + \frac{1}{2}\int_\Omega \boldsymbol{\sigma}[\boldsymbol{\xi}^{k-2}] : \boldsymbol{\epsilon}[\boldsymbol{\xi}]\,dx - \rho\int_\Omega \boldsymbol{f}^{k-1}\cdot\boldsymbol{\xi}\,dx
\end{aligned}$$

Now the second, the fifth and last terms of the above equation are clearly weakly continuous. Hence it is enough to show that weakly lower semi–continuity of the functional

$$\mathcal{I}(\boldsymbol{\xi}) := \int_\Omega |\boldsymbol{\xi}|^2\,dx + \int_\Omega \boldsymbol{\sigma}[\boldsymbol{\xi}] : \boldsymbol{\epsilon}[\boldsymbol{\xi}]\,dx.$$

To show it, let $\{\boldsymbol{\xi}_n\}_{n\in\mathbb{N}} \subset W^{1,2}(\Omega;\mathbb{R}^2)$; $\boldsymbol{\xi}_n \rightharpoonup \boldsymbol{\xi}$ in $W^{1,2}(\Omega;\mathbb{R}^2)$ as $n \to \infty$ be arbitrary weakly converging sequence.

$$\begin{aligned}
0 &\leq \mathcal{I}(\boldsymbol{\xi}_n - \boldsymbol{\xi}) \\
&= \mathcal{I}(\boldsymbol{\xi}_n) - 2\int_\Omega \boldsymbol{\xi}\cdot\boldsymbol{\xi}_n\,dx + \int_\Omega |\boldsymbol{\xi}|^2\,dx - 2\int_\Omega \boldsymbol{\sigma}[\boldsymbol{\xi}] : \boldsymbol{\epsilon}[\boldsymbol{\xi}_n]\,dx + \int_\Omega \boldsymbol{\sigma}[\boldsymbol{\xi}] : \boldsymbol{\epsilon}[\boldsymbol{\xi}]\,dx \\
\mathcal{I}(\boldsymbol{\xi}) &\leq \mathcal{I}(\boldsymbol{\xi}_n) - 2\int_\Omega \boldsymbol{\xi}\cdot(\boldsymbol{\xi}_n - \boldsymbol{\xi})\,dx - 2\int_\Omega \boldsymbol{\sigma}[\boldsymbol{\xi}] : \boldsymbol{\epsilon}[\boldsymbol{\xi}]\,dx \\
\mathcal{I}(\boldsymbol{\xi}) &\leq \liminf_{n\to\infty} \mathcal{I}(\boldsymbol{\xi}_n).
\end{aligned}$$

In the end, $W^{1,2}(\Omega;\mathbb{R}^2)$, $\mathcal{K}^k$ and $\mathcal{J}^k$ satisfy all the hypothesis of Theorem 3. □

4.4 Numerical method for solving the minimization problem

The aim is to minimize $\mathcal{J}^k$ over $\mathcal{K}^k$ numerically using the finite element method.

Given a space discretization parameter $\Delta x > 0$, the domain Ω is approximated by a triangular mesh giving a numerical domain $\widetilde{\Omega}$. We first distribute equispaced nodes of distance approximately Δx on Γ_D and Γ_C and then we generate the interior nodes by applying the Poisson disk sampling algorithm due to [4] with parameter $r = \frac{2}{3}\Delta x$. The triangular mesh is then given by the Delaunay triangulation [25] on the constructed nodes.

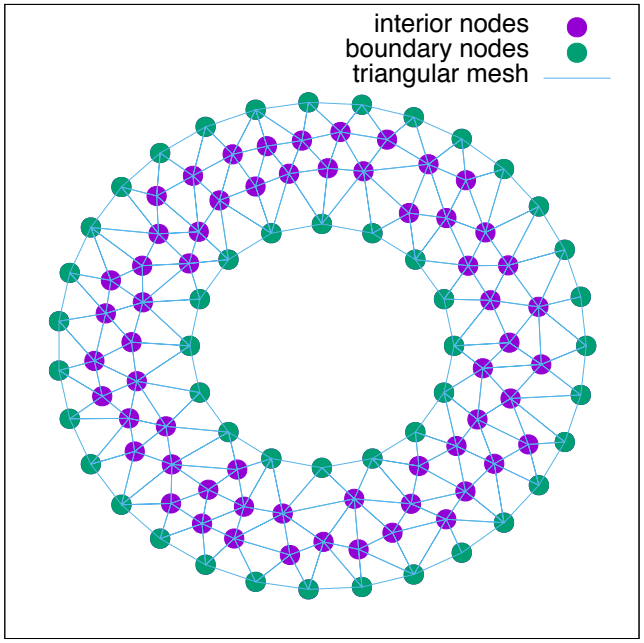

Figure 4.1: Sketch of a numerical domain $\widetilde{\Omega}$

We approximate the minimizer of $\mathcal{J}^k$ by a continuous function on $\widetilde{\Omega}$ that is linear on each element of the mesh. We denote the space of such functions V. Let $N \in \mathbb{N}$ be the number of the nodes, $\{\boldsymbol{x}_n\}_{n=1}^N$ be the nodes, and I_D and I_C be defined

$$I_D := \{n; \boldsymbol{x}_n \in \Gamma_D\}, \quad I_C := \{n; \boldsymbol{x}_n \in \Gamma_C\}. \tag{4.11}$$

We define the basis functions $\zeta_n : \mathbb{R}^2 \to \mathbb{R}$ as the continuous functions, linear on each element, satisfying

$$\zeta_n(\boldsymbol{x}_m) = \delta_{nm}. \tag{4.12}$$

For the vector

$$\widetilde{\boldsymbol{\xi}} = (\widetilde{\xi}_{1,1}, \widetilde{\xi}_{1,2}, \cdots, \widetilde{\xi}_{1,N}, \widetilde{\xi}_{2,1}, \cdots, \widetilde{\xi}_{2,N}) \in \mathbb{R}^{2N},$$

we define the operator $P : \mathbb{R}^{2N} \to V$ as

$$P(\widetilde{\boldsymbol{\xi}})(\boldsymbol{x}) := \left(\sum_{n=1}^N \widetilde{\xi}_{1,n} \zeta_n(\boldsymbol{x}), \sum_{n=1}^N \widetilde{\xi}_{2,n} \zeta_n(\boldsymbol{x}) \right). \tag{4.13}$$

We set $\widetilde{\boldsymbol{\xi}}^0, \widetilde{\boldsymbol{\xi}}^{-1} \in \mathbb{R}^{2N}$ as

$$\widetilde{\xi}^0_{d,n} := \xi^0_d(\boldsymbol{x}_n), \quad \widetilde{\xi}^{-1}_{d,n} := \xi^{-1}_d(\boldsymbol{x}_n), \tag{4.14}$$

for $d = 1, 2$, $n = 1, 2, \cdots, N$. Then for any $k = 1, 2, \cdots, M$, we seek inductively a minimizer $\widetilde{\boldsymbol{\xi}}^k$ of the discrete functional

$$\begin{aligned} \widetilde{\mathcal{J}}^k(\widetilde{\boldsymbol{\xi}}) := \rho \int_{\widetilde{\Omega}} & \frac{\left| P(\widetilde{\boldsymbol{\xi}}) - 2P(\widetilde{\boldsymbol{\xi}}^{k-1}) + P(\widetilde{\boldsymbol{\xi}}^{k-2}) \right|^2}{2(\Delta t)^2} \, dx \\ & + \frac{1}{2} \int_{\widetilde{\Omega}} \left(\frac{1}{2} \boldsymbol{\sigma}[P(\widetilde{\boldsymbol{\xi}})] + \boldsymbol{\sigma}[P(\widetilde{\boldsymbol{\xi}}^{k-2})] \right) : \boldsymbol{\epsilon}[P(\widetilde{\boldsymbol{\xi}})] \, dx \\ & - \rho \int_{\widetilde{\Omega}} \boldsymbol{f} \left((k-1)\Delta t, \cdot, P(\widetilde{\boldsymbol{\xi}}^{k-1}), (P(\widetilde{\boldsymbol{\xi}}^{k-1}) - P(\widetilde{\boldsymbol{\xi}}^{k-2}))/\Delta t \right) \cdot P(\widetilde{\boldsymbol{\xi}}) \, dx, \end{aligned} \tag{4.15}$$

over the admissible set

$$\widetilde{\mathcal{K}}^k := \left\{ \widetilde{\boldsymbol{\xi}} \in \mathbb{R}^{2N}; \widetilde{\xi}_{1,n} = \widetilde{\xi}_{2,n} = 0 \text{ for } n \in I_D, (\boldsymbol{x}_n + (\widetilde{\xi}_{1,n}, \widetilde{\xi}_{2,n})) \cdot \left(\boldsymbol{R}^T(\theta^k) \boldsymbol{e}_2 \right) \geq g^k \text{ for } n \in I_C \right\}. \tag{4.16}$$

For fixed $k \geq 1$, we approximate the minimizer of the functional $\widetilde{\mathcal{J}}^k$ in the admissible set $\widetilde{\mathcal{K}}^k$ using a variant of the nonlinear conjugate gradient method with a projection given by the following steps ($\varepsilon > 0$ is a given stopping tolerance):

(1) initial guess $\widetilde{\boldsymbol{\xi}}_0 \in \widetilde{\mathcal{K}}^k$ (for example, $\widetilde{\boldsymbol{\xi}}_0 = \mathrm{Proj}_{\widetilde{\mathcal{K}}^k}(\widetilde{\boldsymbol{\xi}}^{k-1})$)

(2) $\boldsymbol{g}_1 = -\nabla \widetilde{\mathcal{J}}^k(\widetilde{\boldsymbol{\xi}}_0)$

(3) $\boldsymbol{p}_1 = T^k_{\widetilde{\boldsymbol{\xi}}_0}(\boldsymbol{g}_1)$

(4) $e = \|\boldsymbol{p}_1\|$; if $e \leq \varepsilon$ then set $\widetilde{\boldsymbol{\xi}}^k = \widetilde{\boldsymbol{\xi}}_0$ and proceed to next time step $k+1$

(5) For $m = 1, 2, \ldots$:

(i) $\alpha_m = \mathrm{argmin}_{\alpha>0} \widetilde{\mathcal{J}}^k(\widetilde{\boldsymbol{\xi}}_{m-1} + \alpha \boldsymbol{p}_m)$ (Exact solution as the function is quadratic.)

(ii) $\widetilde{\boldsymbol{\xi}}_m = \mathrm{Proj}_{\widetilde{\mathcal{K}}^k}(\widetilde{\boldsymbol{\xi}}_{m-1} + \alpha_m \boldsymbol{p}_m)$

(iii) $\boldsymbol{g}_{m+1} = -\nabla \widetilde{\mathcal{J}}^k(\widetilde{\boldsymbol{\xi}}_m)$

(iv) $\beta_m = \max\left\{0, \frac{(\boldsymbol{g}_{m+1} - \boldsymbol{g}_m) \cdot \boldsymbol{g}_{m+1}}{\|\boldsymbol{g}_m\|^2}\right\}$

(v) $\boldsymbol{p}_{m+1} = T^k_{\widetilde{\boldsymbol{\xi}}_m}(\boldsymbol{g}_{m+1} + \beta_m \boldsymbol{p}_m)$

(vi) $e = \|T^k_{\widetilde{\boldsymbol{\xi}}_m}(\boldsymbol{g}_{m+1})\|$; if $e \le \varepsilon$ then set $\widetilde{\boldsymbol{\xi}}^k = \widetilde{\boldsymbol{\xi}}_m$ and proceed to next time step $k+1$

where

$$\left(\mathrm{Proj}_{\widetilde{\mathcal{K}}^k}(\widetilde{\boldsymbol{\xi}})\right)_{(n,n+N)} := \begin{cases} (\widetilde{\xi}_{1,n}, \widetilde{\xi}_{2,n}) - \min\left\{0, g^k - (\boldsymbol{x}_n + (\widetilde{\xi}_{1,n}, \widetilde{\xi}_{2,n})) \cdot (\boldsymbol{R}^T(\theta^k)\boldsymbol{e}_2)\right\} (\boldsymbol{R}^T(\theta^k)\boldsymbol{e}_2) & \text{if } n \in I_C, \\ (\widetilde{\xi}_{1,n}, \widetilde{\xi}_{2,n}) & \text{otherwise} \end{cases}$$

for any $\widetilde{\boldsymbol{\xi}} \in \mathbb{R}^{2N}$ and

$$\left(T^k_{\widetilde{\boldsymbol{\xi}}}(\boldsymbol{p})\right)_{(n,n+N)} := \begin{cases} (p_{1,n}, p_{2,n}) - \min\left\{0, (p_{1,n}, p_{2,n}) \cdot (\boldsymbol{R}^T(\theta^k)\boldsymbol{e}_2)\right\} (\boldsymbol{R}^T(\theta^k)\boldsymbol{e}_2) \\ \qquad \text{if } n \in I_C,\ (\boldsymbol{x}_n + (\widetilde{\xi}_{1,n}, \widetilde{\xi}_{2,n})) \cdot (\boldsymbol{R}^T(\theta^k)\boldsymbol{e}_2) \le g^k, \\ (p_{1,n}, p_{2,n}) \qquad \text{otherwise,} \end{cases}$$

for any $\boldsymbol{p} \in \mathbb{R}^{2N}$. The operator $\mathrm{Proj}_{\widetilde{\mathcal{K}}^k}$ is the orthogonal projection onto the set $\widetilde{\mathcal{K}}^k$. The operator $T^k_{\widetilde{\boldsymbol{\xi}}}(\boldsymbol{p})$ restricts the search direction $(\boldsymbol{p})_{(n,n+N)}$ for $n \in I_C$ so as not to jump over the obstacle g^k.

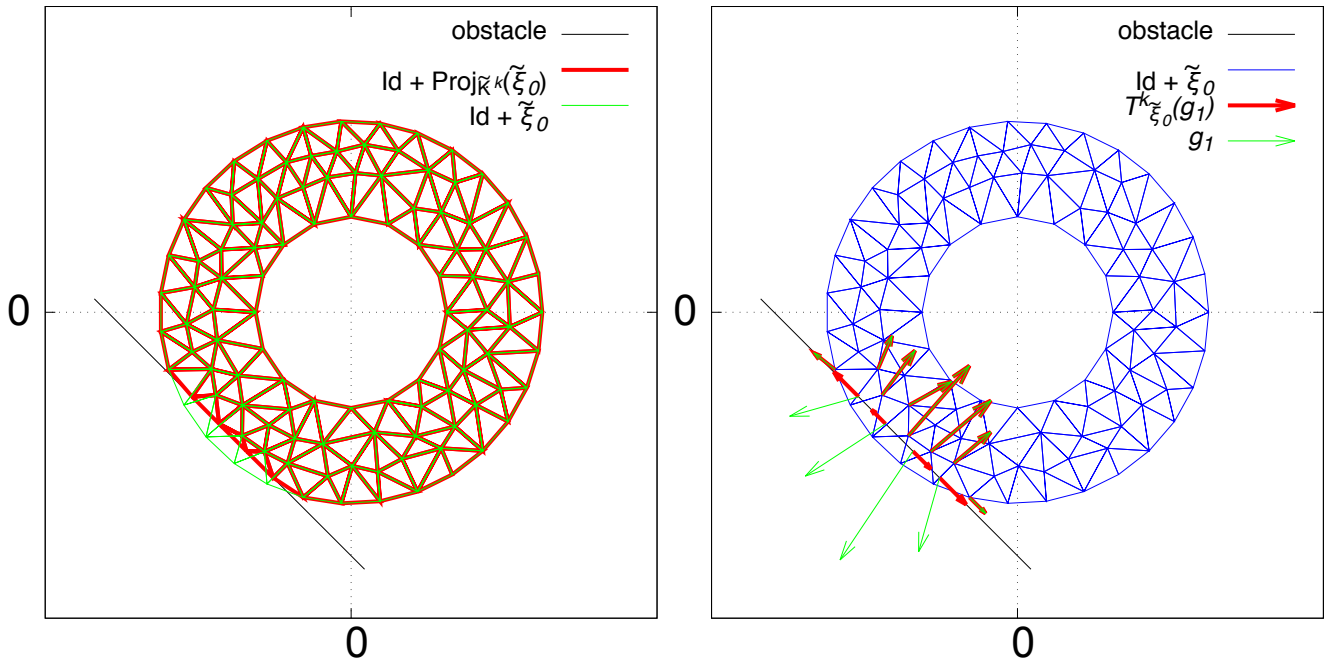

Figure 4.2: Sketch of the operator $\mathrm{Proj}_{\widetilde{\mathcal{K}}^k}$ and $T^k_{\widetilde{\boldsymbol{\xi}}}$

Chapter 5

Numerical results

In this section we present numerical results based on the method proposed in Chapter 4. We choose the domain Ω as the annulus

$$\Omega := \{\boldsymbol{x} \in \mathbb{R}^2; r_D < |\boldsymbol{x}| < r_C\}, \quad \Gamma_D := \{\boldsymbol{x} \in \mathbb{R}^2; |\boldsymbol{x}| = r_D\}, \quad \Gamma_C := \{\boldsymbol{x} \in \mathbb{R}^2; |\boldsymbol{x}| = r_C\},$$

where $r_D = 0.25$ and $r_C = 0.5$. We further set the initial data as $\boldsymbol{\xi}^0 = \mathbf{0}$ and $\boldsymbol{\eta}^0 = \mathbf{0}$. The Lamé constants are given by

$$\lambda = \frac{E\nu}{(1+\nu)(1-2\nu)}, \quad \mu = \frac{E}{2(1+\nu)},$$

where E and ν are Young's modulus and Poisson's ratio, respectively. We set Δx as the mesh size. Table 5.1 shows the reference values of the involved parameters.

E	ν	ρ	ω	Δx
0.1	0.49	1	$\pi/10$	0.0125

Table 5.1: Reference values for the parameters involved in the simulations.

We simulate two cases. In the first case we remove the obstacle, and study the sensitivity of the roller's dynamics with respect to the parameters. In particular, we are interested in the vibrations in the radial and tangential displacements, because the understanding of these vibrations might help in removing the squeaking sound of printer rollers. As feedback on these simulations, we add a vibration to the given rotation $\theta(t)$ to investigate the occurrence of resonance.

In the second case we add the obstacle. We are interested in the shape of the deformed domain and the size of the stress tensor $\boldsymbol{\sigma}[\boldsymbol{\xi}]$ as a function on the deformed domain, especially in the region close to the contact zone.

5.1 The case without an obstacle

We set g small enough to remove any effect from the obstacle. We are interested in the average radial displacement R and the average tangential displacement α of the roller defined by

$$R(t) = \frac{1}{|\Gamma_C|} \int_{\Gamma_C} \frac{\boldsymbol{\xi}(\boldsymbol{x}, t) \cdot \boldsymbol{x}}{|\boldsymbol{x}|} \, ds, \tag{5.1}$$

$$\alpha(t) = \frac{1}{|\Gamma_C|} \int_{\Gamma_C} \frac{\boldsymbol{\xi}(\boldsymbol{x}, t) \cdot \boldsymbol{x}^{\perp}}{|\boldsymbol{x}|} \, ds. \tag{5.2}$$

We set the parameter values as in Table 5.1 unless mentioned otherwise.

In the first set of simulations, we consider the four values $\Delta x = \Delta x_i := 2^{i-1}\Delta\widetilde{x}$ for $i = 1, 2, \cdots, 4$, $\Delta\widetilde{x} := 0.0125$ and set the corresponding time step size as $\Delta t = \Delta x$. We consider a linear time-dependence for the rotation angle given by

$$\theta(t) = \omega t. \tag{5.3}$$

Figures 5.1 and 5.2 show the corresponding graphs of $R(t)$ and $\alpha(t)$, which resemble waves. These should correspond to the vibration modes in the radial and tangential directions, see [2]. We can estimate the periods of the first modes by assuming that the roller can be approximated by a infinite strip of thickness $d = r_C - r_D$ of an elastic material whose one side is fixed (boundary Γ_D) and the other is free to move (boundary Γ_C). The first mode then has wavelength $\Lambda \approx 4d$. The wavelength is related to the period τ as $\Lambda = c\tau$, where c is the speed of sound. Elastic material has primary (pressure) and secondary (shear) waves with speeds

$$c_p = \sqrt{\frac{\lambda + 2\mu}{\rho}}, \qquad c_s = \sqrt{\frac{\mu}{\rho}}, \tag{5.4}$$

which yields for our parameters

$$\tau_p = \frac{4d}{c_p} \approx 0.764, \qquad \tau_s = \frac{4d}{c_s} \approx 5.46.$$

The short period waves therefore correspond to the radial vibration mode (primary wave) and the long period waves correspond to the tangential vibration mode (secondary wave). The radial vibration is initiated by the centrifugal force. Once there is a motion in the radial direction, the Coriolis effect causes the tangential vibration.

Firstly, we observe that the amplitude of the waves does not change in time. We expect this from Theorem 1, which shows in a simplified setting that the time-discrete energy is conserved. Secondly, we observe a phase-shift when Δx varies. The phase-shift decreases as Δx decreases. It is curious that the phase shift of $\alpha(t)$ is much higher than the phase shift of $R(t)$; we did not find an explanation for this effect.

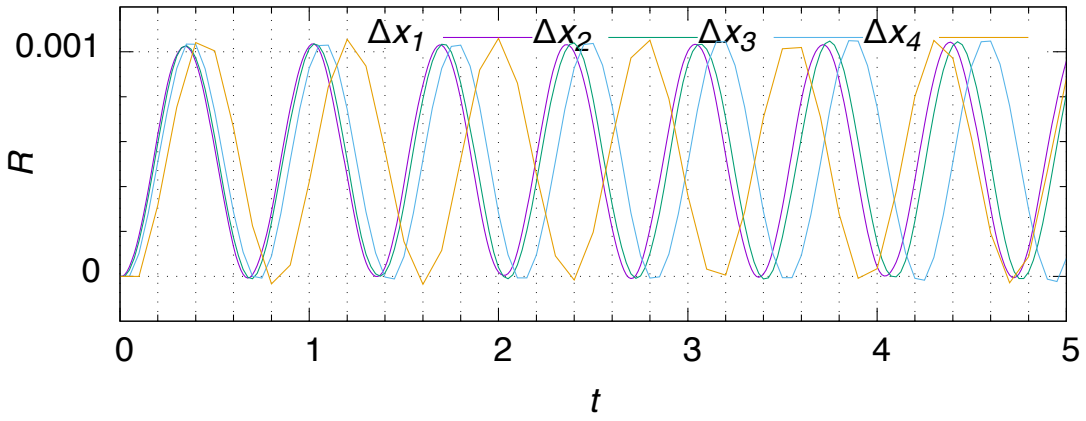

Figure 5.1: The average radial displacement $R(t)$ (see (5.1)) as a function of time for four values of the mesh size Δx.

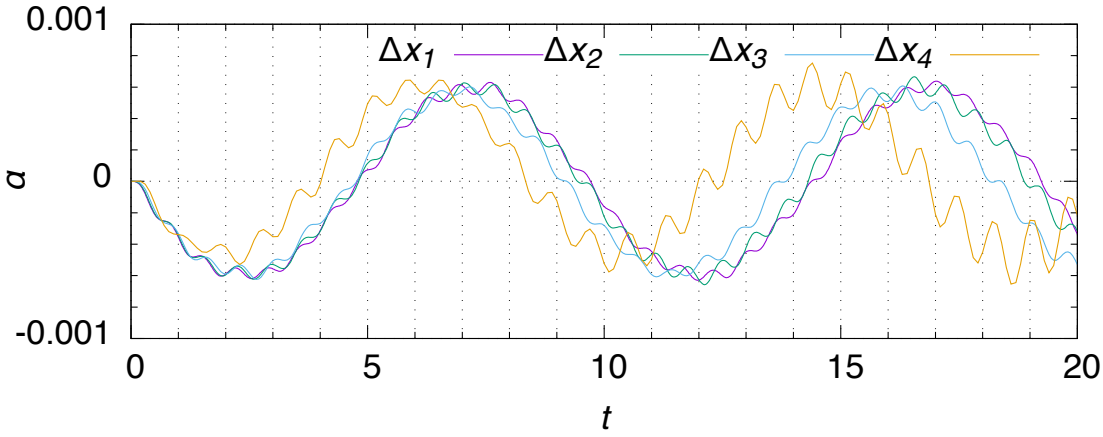

Figure 5.2: The average tangential displacement $\alpha(t)$ (see (5.2)) as a function of time for four values of the mesh size Δx.

In the next set of simulations, we vary Young's modulus by $E = E_i := 2^{i-1}\widetilde{E}$ $(i = 1, 2, \cdots, 4\widetilde{E} := 0.05)$ instead. Figures 5.3 and 5.4 show the graphs of $R(t)$ and $\alpha(t)$ again. Firstly, we observe that the amplitude of the wave of $R(t)$ is halved when E is doubled, which is expected from the physical meaning of Young's modulus. Secondly, the frequency of the wave of $R(t)$ seems to scale as the square root of E, which we expect from (5.4). Thirdly, we observe that the amplitude of the wave of $\alpha(t)$ decreases when E increases. Indeed, since the amplitude of the radial wave decreases with increasing E and the tangential vibration is caused by the Coriolis effect whose magnitude depends on the radial velocity, as discussed above, this is the expected behavior. Finally, the frequency of the wave of $\alpha(t)$ seems to scale as the square root of E, which we expect from (5.4).

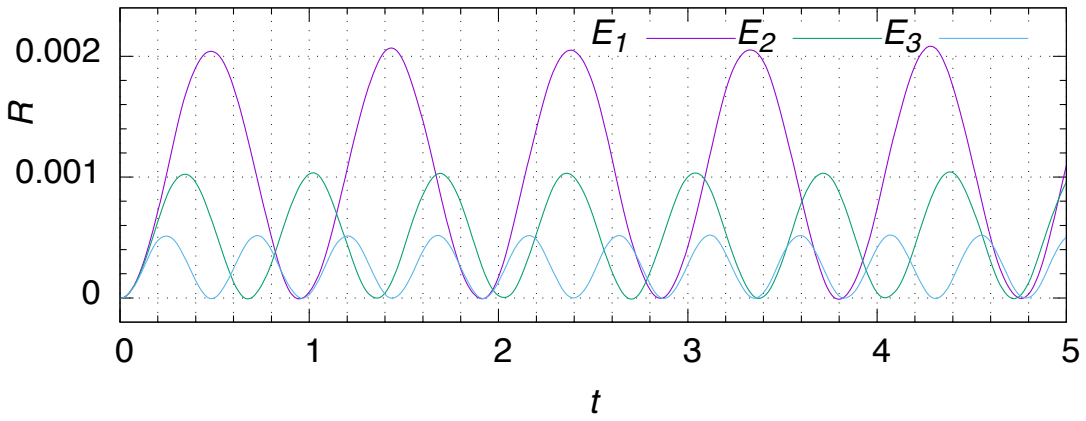

Figure 5.3: The graph of $R(t)$ for three values of Young's modulus E.

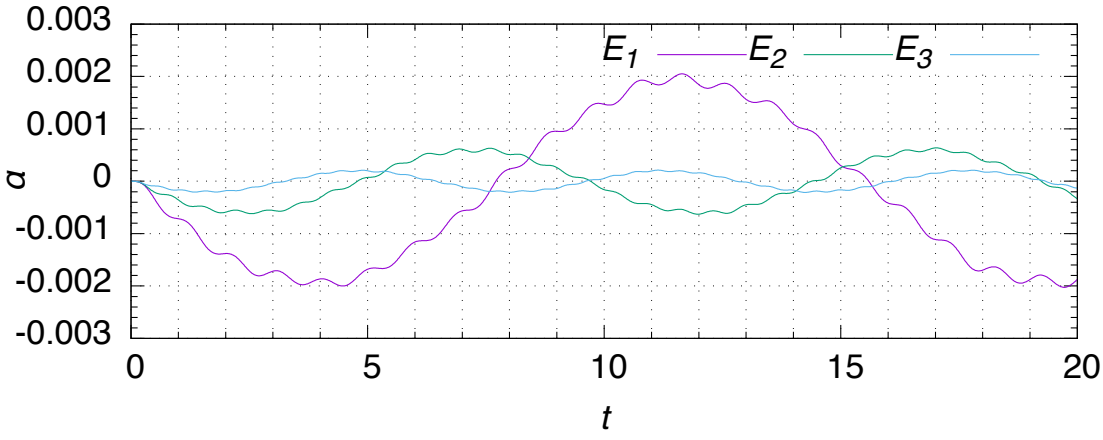

Figure 5.4: The graph of $\alpha(t)$ for three values of Young's modulus E.

In the case that Young's modulus is smaller, Figure 5.5 and 5.6 show that the value of R and α do not come back to the zero in time. Moreover, Figure 5.7 and 5.8 show that similar results are obtained when the thickness $d = r_C - r_D$ is double.

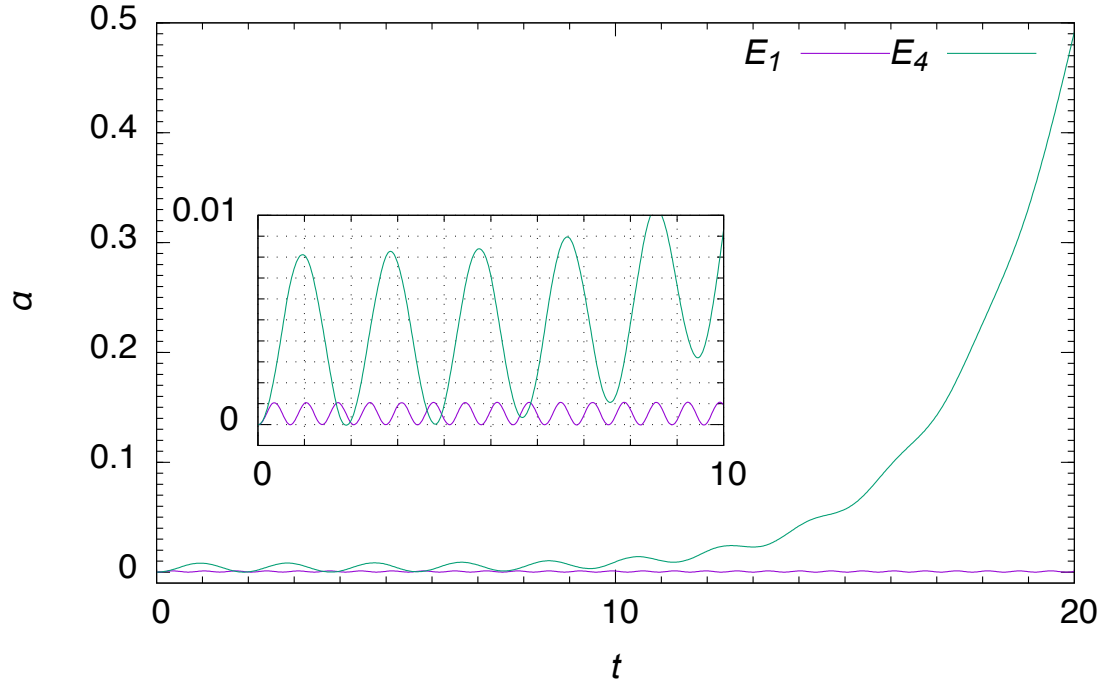

Figure 5.5: The graph of $R(t)$ for two values of Young's modulus E.

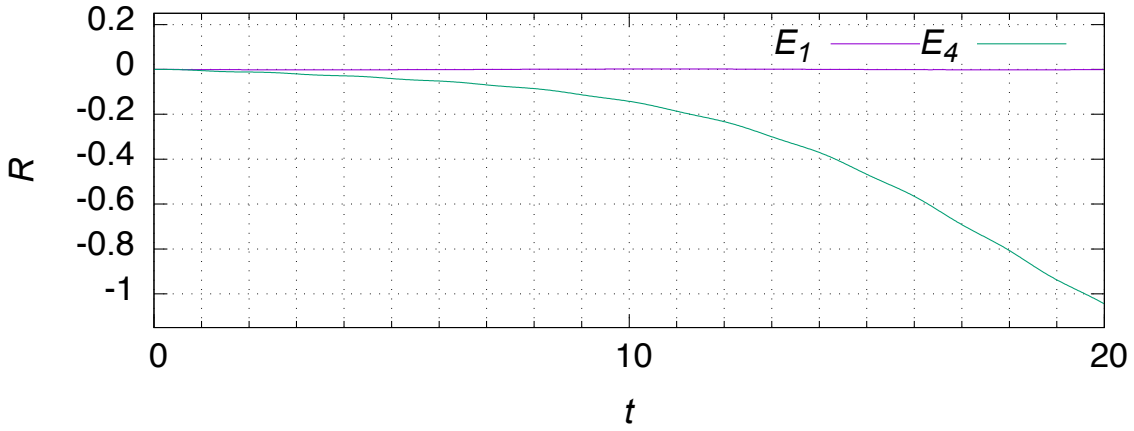

Figure 5.6: The graph of $\alpha(t)$ for two values of Young's modulus E.

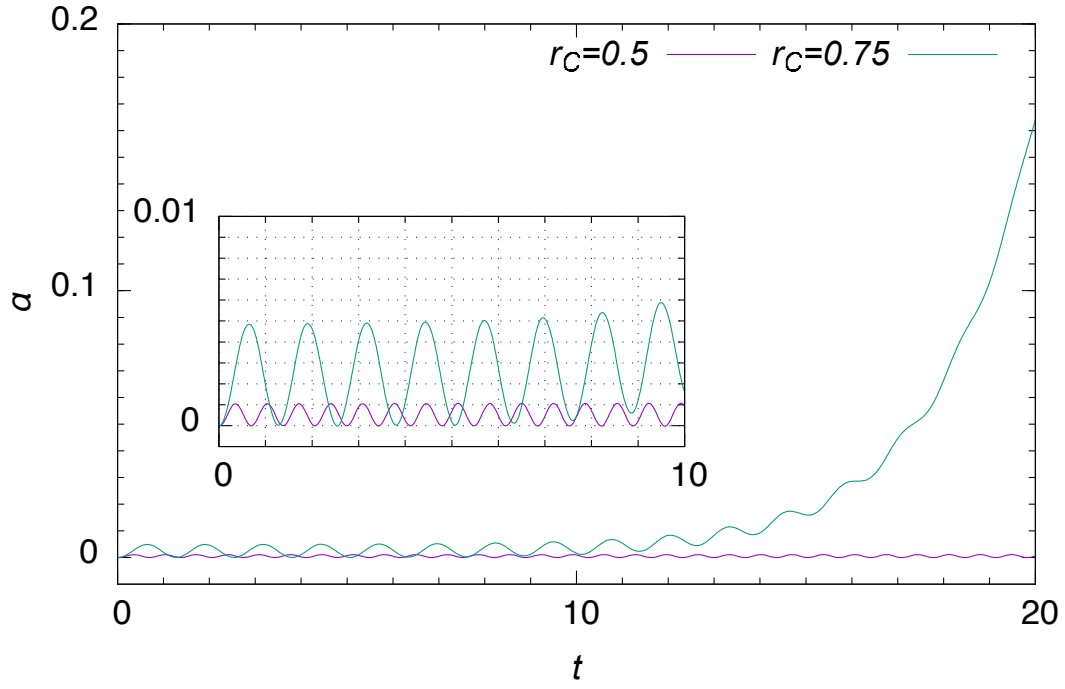

Figure 5.7: The graph of $R(t)$ for two values of the radius r_C.

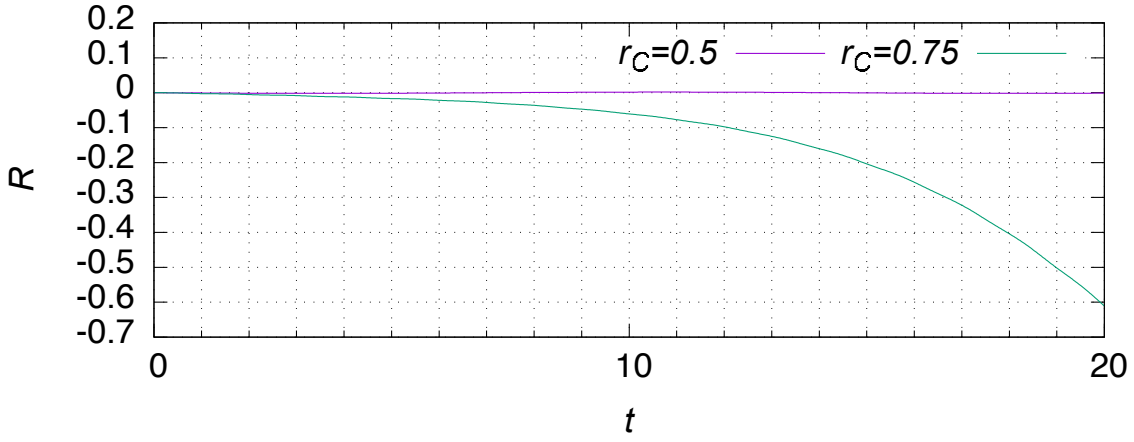

Figure 5.8: The graph of $\alpha(t)$ for three values of the radius r_C.

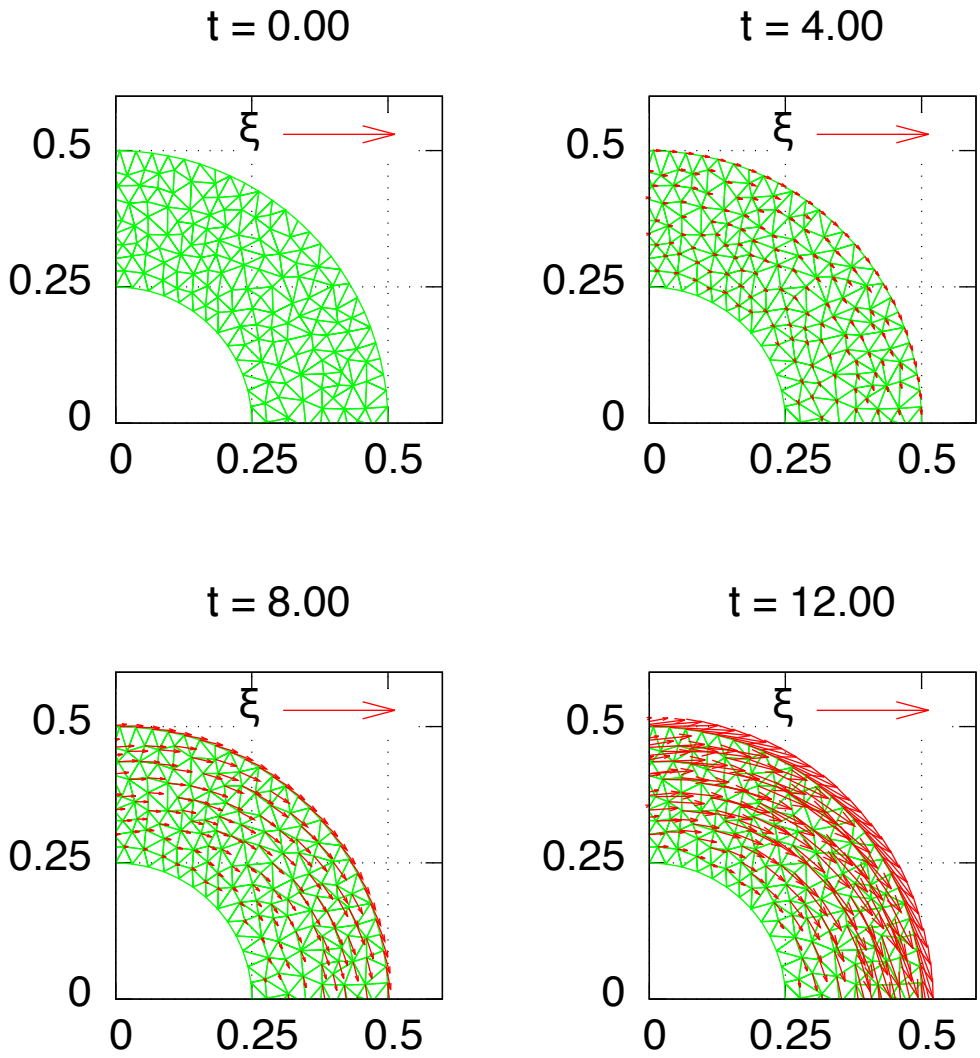

Figure 5.9: Reference domain/The red vectors display $\boldsymbol{\xi}$. Young's modulus $E = E_4$.

In the final simulation for the roller without obstacle, we try to enforce resonance by perturbing the rotation angle by a wave, i.e., we set

$$\theta(t) = \omega t + a\cos(bt). \tag{5.5}$$

Based on Figure 5.4, the period of α is 9.75 approximately when $E = E_2$. We set $b = 2\pi/9.75$ for the frequency of the perturbation in Figure 5.10. We choose $a = 0.001$ for the amplitude to ensure that the perturbation only amounts to a small contribution to $\dot{\theta}(t)$. Figure 5.10 shows the resulting graph of $\alpha(t)$. Even though the perturbation is small, we observe a significant increase in the amplitude of $\alpha(t)$ over time. Such resonance effect can be the key for understanding the squeaking sound of rollers.

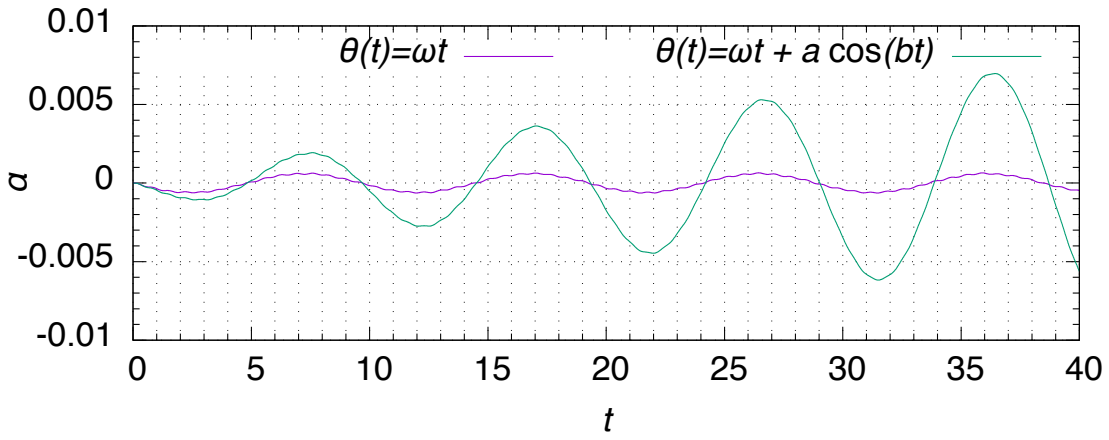

Figure 5.10: The graph of $\alpha(t)$ for the perturbed rotation given by (5.5). The graph in Figure 5.2 is repeated here for reference.

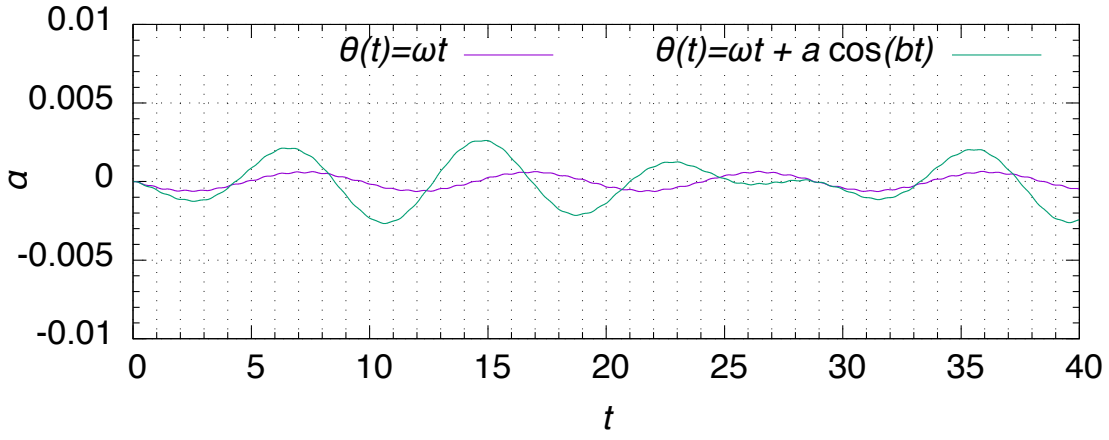

Figure 5.11: The graph of $\alpha(t)$ for the perturbed rotation given by (5.5). The graph in Figure 5.2 is repeated here for reference. We set $b = 7.25$.

5.2 The case with an obstacle

We set the height of the obstacle g as

$$g(t) = \min\left\{0.005t, \frac{r_C - r_D}{10}\right\} - r_C. \tag{5.6}$$

With the choice, at $t = 0$, the contact zone between the obstacle and the deformed configuration consists of a single point. Then, the obstacle compresses the roller by moving upwards with constant velocity until the time t at which $g(t) = \frac{r_C - r_D}{10} - r_C$. From this time t onwards, g remains constant in time.

It turns out that the obstacle creates high frequency waves in the stress field in Ω. To

suppress these waves, we add a damping term to the energy functional $\mathcal{J}^k$:

$$\mathcal{J}_\eta^k(\boldsymbol{\xi}) := \mathcal{J}^k(\boldsymbol{\xi}) + \eta \int_\Omega \frac{|\boldsymbol{\xi} - \boldsymbol{\xi}^{k-2}|^2}{4\Delta t}\, dx, \tag{5.7}$$

where we set $\eta = 1$. The corresponding change to $(\mathrm{P_k})$ is that the first equation is replaced by

$$\rho\ddot{\boldsymbol{\xi}} + \eta\dot{\boldsymbol{\xi}} = \mathbf{div}\boldsymbol{\sigma}[\boldsymbol{\xi}] + \rho\boldsymbol{f}(\cdot, \cdot, \boldsymbol{\xi}, \dot{\boldsymbol{\xi}}) \quad \text{ in } \Omega \times (0, T). \tag{5.8}$$

Figure 5.12 and 5.13 illustrate the magnitude of the stress defined by

$$|\boldsymbol{\sigma}| := \sqrt{\sum_{ij} \sigma_{ij}^2}, \tag{5.9}$$

on the deformed configuration. In the simulations, we consider the two values $\omega = 0, \pi/10$. Figure 5.12 illustrates the simple compression. The shock of the contact of the obstacle propagates symmetrically.

In Figure 5.13, we observe that the stress is initially concentrated near the boundary Γ_D; this is natural for Dirichlet boundary conditions. The shock propagates more rapidly in the direction of the rotation. We conjecture that the complicated stress distribution at $t = 5$ is caused by the interaction of the radial waves (see Figures 5.1 and 5.3) with the forced compression by the obstacle.

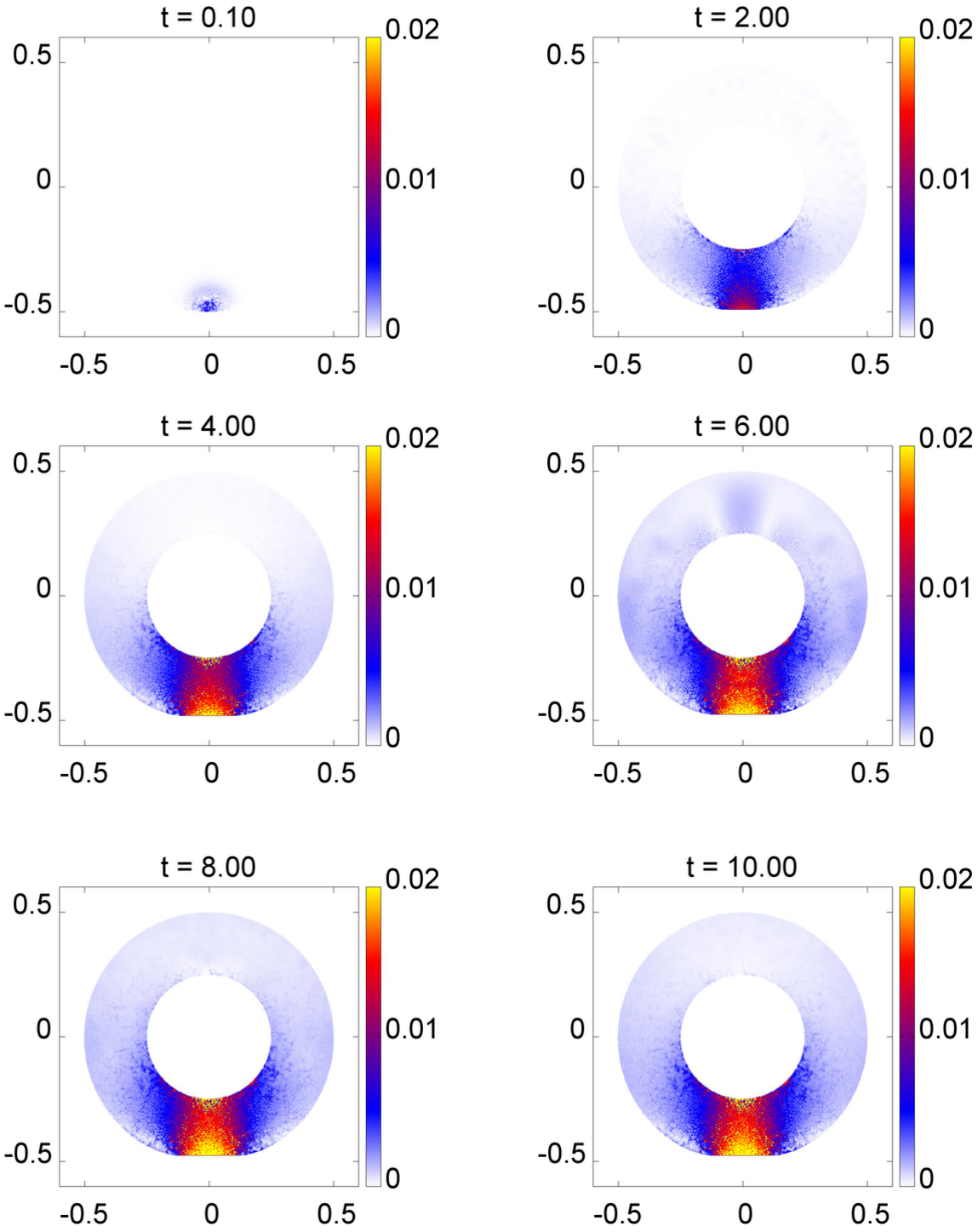

Figure 5.12: Simple compression ($\omega = 0$). Here, the magnitude of the stress (see (5.9)) is displayed.

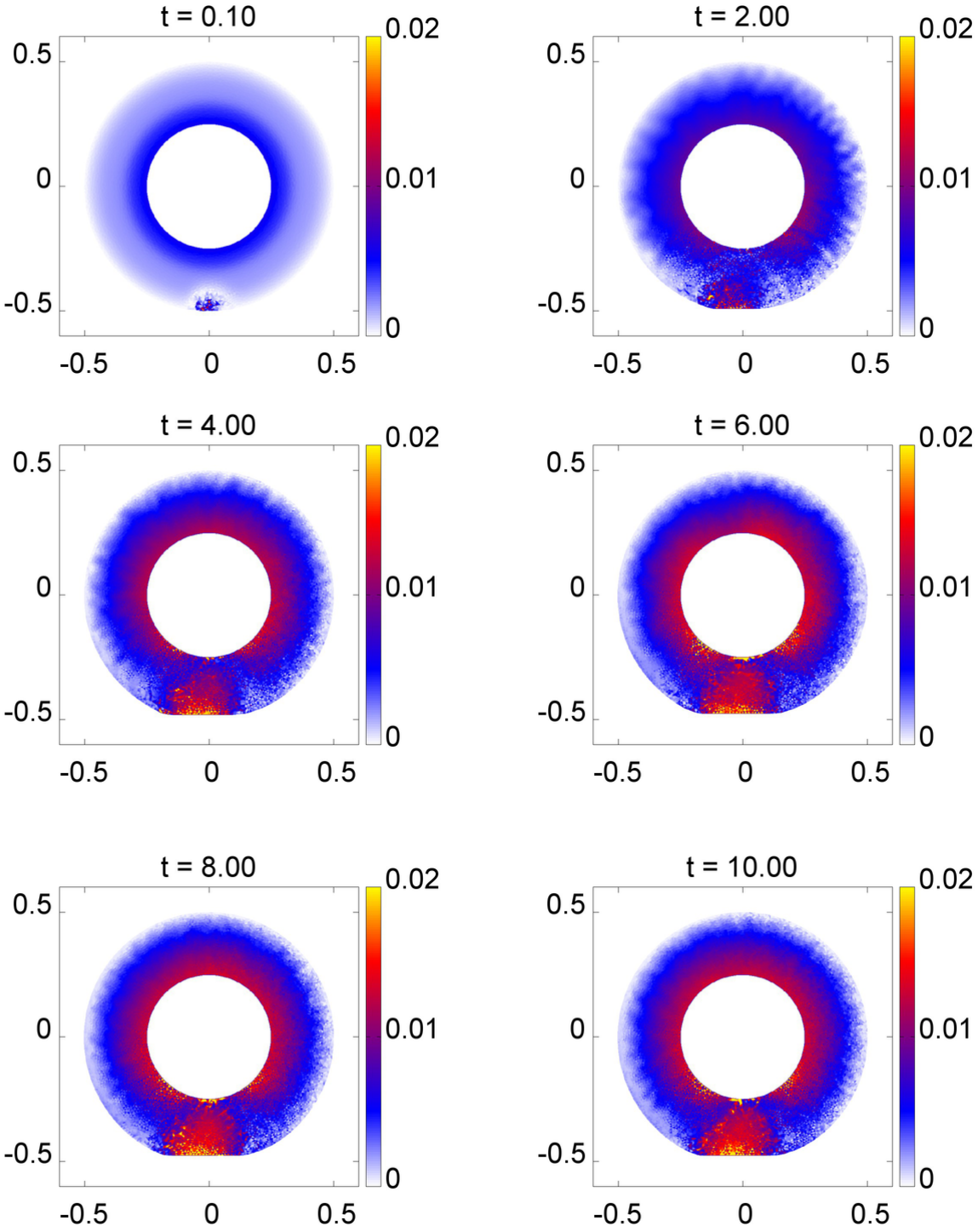

Figure 5.13: The direction of rotation is counter-clockwise with the rotation speed $\omega = \pi/10$. The magnitude of the stress (see (5.9)) is displayed.

Chapter 6

Discrete Morse flow

6.1 Construction of weak solution for a linear elasticity problem

Let $\Omega \subset \mathbb{R}^d$ be a bounded domain representing the area occupied by an elastic body. We denote by $\boldsymbol{u} : \overline{\Omega} \to \mathbb{R}^d$ the displacement of the domain $\overline{\Omega}$,

We shall consider the conservation of linear momentum with the homogeneous Dirichlet boundary condition and initial conditions $\boldsymbol{u}^0$ and $\boldsymbol{v}^0$ as follows:

$$\rho \ddot{\boldsymbol{u}} = \mathbf{div}\, \boldsymbol{\sigma}[\boldsymbol{u}] \qquad \text{in} \quad \Omega \times (0,T) =: Q_T \tag{6.1}$$

$$\boldsymbol{u} = \mathbf{0} \qquad \text{on} \quad \partial\Omega \times [0,T) \tag{6.2}$$

$$\boldsymbol{u}(\cdot,0) = \boldsymbol{u}^0 \qquad \text{in} \quad \Omega, \tag{6.3}$$

$$\dot{\boldsymbol{u}}(\cdot,0) = \boldsymbol{v}^0 \qquad \text{in} \quad \Omega, \tag{6.4}$$

where $\rho > 0$ is the density, superposed dots denote partial differentiation with respect to time (i.e., $\ddot{\boldsymbol{u}} := \partial^2 \boldsymbol{u}/\partial t^2$).

We explain the details of the discrete Morse flow on the example of the linear elasticity equation (6.1)–(6.4). It is considered in a bounded domain $\Omega \subset \mathbb{R}^d$ with smooth boundary $\partial\Omega$. The initial data $\boldsymbol{u}_0, \boldsymbol{v}_0 \in W_0^{1,2}(\Omega;\mathbb{R}^d)$ are given.

We define the functional $\mathcal{E}$ by

$$\mathcal{E}(\boldsymbol{v}) := \int_\Omega \boldsymbol{\sigma}[\boldsymbol{v}] : \boldsymbol{\epsilon}[\boldsymbol{v}]\, dx, \tag{6.5}$$

for any $\boldsymbol{v} \in W^{1,2}(\Omega;\mathbb{R}^d)$. The functional $\mathcal{E}$ is weakly lower semi continuous in $W_0^{1,2}(\Omega;\mathbb{R}^d)$. Indeed, for arbitrary weakly converging sequence $\{\boldsymbol{u}_n\}_{n\in\mathbb{N}} \subset W_0^{1,2}(\Omega;\mathbb{R}^d)$ and the weak limit

$\boldsymbol{u} \in W_0^{1,2}(\Omega;\mathbb{R}^d)$, we have

$$\begin{aligned}
0 &\le \mathcal{E}(\boldsymbol{u}_n - \boldsymbol{u}) \\
&= \int_\Omega \boldsymbol{\sigma}[\boldsymbol{u}_n] : \boldsymbol{\epsilon}[\boldsymbol{u}_n]\,dx - 2\int_\Omega \boldsymbol{\sigma}[\boldsymbol{u}] : \boldsymbol{\epsilon}[\boldsymbol{u}_n]\,dx + \int_\Omega \boldsymbol{\sigma}[\boldsymbol{u}] : \boldsymbol{\epsilon}[\boldsymbol{u}]\,dx, \\
\mathcal{E}(\boldsymbol{u}) &\le \int_\Omega \boldsymbol{\sigma}[\boldsymbol{u}_n] : \boldsymbol{\epsilon}[\boldsymbol{u}_n]\,dx - 2\int_\Omega \boldsymbol{\sigma}[\boldsymbol{u}] : \boldsymbol{\epsilon}[\boldsymbol{u}_n - \boldsymbol{u}]\,dx \\
&= \int_\Omega \boldsymbol{\sigma}[\boldsymbol{u}_n] : \boldsymbol{\epsilon}[\boldsymbol{u}_n]\,dx - 2\int_\Omega c_{ijpq}\frac{\partial u_p}{\partial x_q}\frac{\partial (\boldsymbol{u}_n - \boldsymbol{u})_i}{\partial x_j}\,dx, \\
\mathcal{E}(\boldsymbol{u}) &\le \liminf_{n\to\infty} \mathcal{E}(\boldsymbol{u}_n).
\end{aligned}$$

Let $M > 0$ be a natural number, $h = T/M$ be the time step. We determine $\boldsymbol{u}^{-1} := \boldsymbol{u}^0 - h\boldsymbol{v}^0$. We define the approximate solution $\boldsymbol{u}^k$ on time levels $t = kh$ for $k = 1, 2, \cdots, M$, to be the minimizer of the following functional in $W_0^{1,2}(\Omega;\mathbb{R}^d)$:

$$\mathcal{J}^k(\boldsymbol{v}) := \frac{1}{2h^2}\left\|\boldsymbol{v} - 2\boldsymbol{u}^{k-1} + \boldsymbol{u}^{k-2}\right\|^2_{L^2(\Omega;\mathbb{R}^d)} + \frac{1}{2}\mathcal{E}(\boldsymbol{v}) \tag{6.6}$$

Lemma 1. *There exists a minimizer of $\mathcal{J}^k$ on $W_0^{1,2}(\Omega;\mathbb{R}^d)$.*

Proof. Since $\mathcal{J}^k$ is bounded from below, there exists $\{\boldsymbol{u}_n\}_{n\in\mathbb{N}} \subset W_0^{1,2}(\Omega;\mathbb{R}^d)$ such that

$$\mathcal{J}^k(\boldsymbol{u}_n) \searrow \inf_{\boldsymbol{v}\in W_0^{1,2}(\Omega;\mathbb{R}^d)} \mathcal{J}^k(\boldsymbol{v}). \tag{6.7}$$

We show the boundedness of $\{\boldsymbol{u}_n\}_{n\in\mathbb{N}}$ in $W^{1,2}(\Omega;\mathbb{R}^d)$. Since there exists $C_P, C_K > 0$ such that

$$\|u_i\|_{L^2(\Omega)} \le C_P \left\|\frac{\partial u_i}{\partial x_j}\right\|_{L^2(\Omega)}, \tag{6.8}$$

$$\int_\Omega \frac{\partial v_i}{\partial x_j}\frac{\partial v_i}{\partial x_j}\,dx \le C_K \int_\Omega \epsilon_{ij}[\boldsymbol{v}]\epsilon_{ij}[\boldsymbol{v}]\,dx, \tag{6.9}$$

for any $\boldsymbol{v} \in W_0^{1,2}(\Omega;\mathbb{R}^d)$ from the Poincaré inequality and Korn inequality, we have

$$\begin{aligned}
\|\boldsymbol{u}_n\|^2_{W^{1,2}(\Omega;\mathbb{R}^d)} &\le (C_P^2+1)\int_\Omega \left|\frac{\partial (\boldsymbol{u}_n)_i}{\partial x_j}\right|^2 dx \\
&\le (C_P^2+1)C_K \int_\Omega \epsilon_{ij}[\boldsymbol{u}_n]\epsilon_{ij}[\boldsymbol{u}_n]\,dx \\
&\le \frac{(C_P^2+1)C_K}{2\mu}\int_\Omega c_{ijpq}\epsilon_{pq}[\boldsymbol{u}_n]\epsilon_{ij}[\boldsymbol{u}_n]\,dx \\
&= \frac{(C_P^2+1)C_K}{\mu}\mathcal{E}(\boldsymbol{u}_n) \\
&\le \frac{(C_P^2+1)C_K}{2\mu}\mathcal{J}^k(\boldsymbol{u}_n) \\
&\le \frac{(C_P^2+1)C_K}{2\mu}\mathcal{J}^k(\boldsymbol{u}_0).
\end{aligned}$$

Therefore there exists subsequence $\{\boldsymbol{u}_{n_j}\}_{j\in\mathbb{N}}$ and $\boldsymbol{u}^k \in W_0^{1,2}(\Omega;\mathbb{R}^d)$ such that

$$\boldsymbol{u}_{n_j} \rightharpoonup \boldsymbol{u}^k \quad \text{in } W^{1,2}(\Omega;\mathbb{R}^d) \quad \text{as } j\to\infty. \tag{6.10}$$

From Rellich-Kondrashov theorem, we take subsequence $\{\boldsymbol{u}_{n_{j_r}}\}_{r\in\mathbb{N}}$ converging to $\boldsymbol{u}^k$ strongly in $L^2(\Omega;\mathbb{R}^d)$. We rewrite the subsequence by $\{\boldsymbol{u}_{n_j}\}_{j\in\mathbb{N}}$ for simplify.

Then $\boldsymbol{u}^k$ is a minimizer of $\mathcal{J}^k$ on $W_0^{1,2}(\Omega;\mathbb{R}^d)$. Indeed, we have

$$\begin{aligned}
\inf_{\boldsymbol{v}\in W_0^{1,2}(\Omega;\mathbb{R}^d)} \mathcal{J}^k(\boldsymbol{v}) &= \liminf_{j\to\infty} \mathcal{J}^k(\boldsymbol{u}_{n_j}) \\
&= \liminf_{j\to\infty} \left\{ \frac{1}{2h^2} \left\| \boldsymbol{u}_{n_j} - 2\boldsymbol{u}^{k-1} + \boldsymbol{u}^{k-2} \right\|^2_{L^2(\Omega;\mathbb{R}^d)} + \mathcal{E}(\boldsymbol{u}_{n_j}) \right\} \\
&= \frac{1}{2h^2} \left\| \boldsymbol{u}^k - 2\boldsymbol{u}^{k-1} + \boldsymbol{u}^{k-2} \right\|^2_{L^2(\Omega;\mathbb{R}^d)} + \liminf_{j\to\infty} \mathcal{E}(\boldsymbol{u}_{n_j}) \\
&\geq \mathcal{J}^k(\boldsymbol{u}^k).
\end{aligned}$$

□

As the next step, we define the approximate solutions $\overline{\boldsymbol{u}}^h$ and $\widehat{\boldsymbol{u}}^h$ interpolated in time with the minimizers $\{\boldsymbol{u}^k\}_{k=-1}^M$.

$$\overline{\boldsymbol{u}}^h(\boldsymbol{x},t) = \boldsymbol{u}^k(\boldsymbol{x}), \qquad t\in((k-1)h,kh], k=0,\cdots,M, \tag{6.11}$$

$$\widehat{\boldsymbol{u}}^h(\boldsymbol{x},t) = \frac{t-(k-1)h}{h}\boldsymbol{u}^k(\boldsymbol{x}) + \frac{kh-t}{h}\boldsymbol{u}^{k-1}(\boldsymbol{x}), \quad t\in((k-1)h,kh], k=0,\cdots,M. \tag{6.12}$$

Since $\boldsymbol{u}^k$ is a minimizer of $\mathcal{J}^k$ on $W_0^{1,2}(\Omega;\mathbb{R}^d)$ for any $\boldsymbol{w}\in W_0^{1,2}(\Omega;\mathbb{R}^d)$ we have

$$\begin{aligned}
0 &= \frac{d}{ds}\mathcal{J}^k(\boldsymbol{u}^k + s\boldsymbol{w})\Big|_{s=0} \\
&= \lim_{s\to0}\frac{1}{s}\left\{\mathcal{J}^k(\boldsymbol{u}^k+s\boldsymbol{w}) - \mathcal{J}^k(\boldsymbol{u}^k)\right\} \\
&= \lim_{s\to0}\frac{1}{2sh^2}\int_\Omega \left(|\boldsymbol{u}^k + s\boldsymbol{w} - 2\boldsymbol{u}^{k-1} + \boldsymbol{u}^{k-2}|^2 - |\boldsymbol{u}^k - 2\boldsymbol{u}^{k-1} + \boldsymbol{u}^{k-2}|^2\right) dx \\
&\quad + \lim_{s\to0}\frac{1}{2s}\int_\Omega \left(\boldsymbol{\sigma}[\boldsymbol{u}^k + s\boldsymbol{w}] : \boldsymbol{\epsilon}[\boldsymbol{u}^k + s\boldsymbol{w}] - \boldsymbol{\sigma}[\boldsymbol{u}^k] : \boldsymbol{\sigma}[\boldsymbol{u}^k]\right) dx \\
&= \lim_{s\to0}\frac{1}{2h^2}\int_\Omega \left(2\boldsymbol{u}^k + s\boldsymbol{w} - 4\boldsymbol{u}^{k-1} + 2\boldsymbol{u}^{k-2}\right)\cdot\boldsymbol{w}\, dx \\
&\quad + \lim_{s\to0}\frac{1}{2}\int_\Omega \left(2\boldsymbol{\sigma}[\boldsymbol{u}^k] : \boldsymbol{\epsilon}[\boldsymbol{w}] + s\boldsymbol{\sigma}[\boldsymbol{w}] : \boldsymbol{\epsilon}[\boldsymbol{w}]\right) dx \\
&= \int_\Omega \frac{\boldsymbol{u}^k - 2\boldsymbol{u}^{k-1} + \boldsymbol{u}^{k-2}}{h^2}\cdot\boldsymbol{w}\, dx + \int_\Omega \boldsymbol{\sigma}[\boldsymbol{u}^k] : \boldsymbol{\epsilon}[\boldsymbol{w}]\, dx
\end{aligned} \tag{6.13}$$

Using (6.11) and (6.12), we rewrite

$$0 = \int_\Omega \frac{1}{h}\left\{\frac{\partial\widehat{\boldsymbol{u}}^h}{\partial t}(t) - \frac{\partial\widehat{\boldsymbol{u}}^h}{\partial t}(t-h)\right\}\cdot\boldsymbol{w}\, dx + \int_\Omega \boldsymbol{\sigma}[\overline{\boldsymbol{u}}^h(t)] : \boldsymbol{\epsilon}[\boldsymbol{w}]\, dx, \tag{6.14}$$

for almost everywhere $t\in(0,T)$, for any $\boldsymbol{w}\in W_0^{1,2}(\Omega;\mathbb{R}^d)$.

Lemma 2. *Suppose Ω is a bounded domain with smooth boundary. Let $\mathcal{J}^k$, $k = 1, 2, \cdots, M$, be the functionals defined by* (6.6) *and let $\boldsymbol{u}^k$ be corresponding minimizers in $W_0^{1,2}(\Omega; \mathbb{R}^d)$. Define functions $\overline{\boldsymbol{u}}^h$ and $\widehat{\boldsymbol{u}}^h$ by* (6.11) *and* (6.12) *and assume $h \leq 1$. Then the following estimate holds*

$$\left\| \frac{\partial \widehat{u}_i^h}{\partial t}(t) \right\|_{L^2(\Omega)} + \left\| \frac{\partial \overline{u}_i^h}{\partial x_j}(t) \right\|_{L^2(\Omega)} \leq C_E \qquad \text{for a.e. } t \in (0, T), \tag{6.15}$$

where constant C_E depend on $W_0^{1,2}$-norms of the initial data but is independent of h.

Proof. We substitute $\boldsymbol{w} = \boldsymbol{u}^k - \boldsymbol{u}^{k-1}$ into (6.13). Using the inequality $(a-b)a \geq a^2/2 - b^2/2$ for $a, b \in \mathbb{R}$, we get

$$\begin{aligned}
0 &= \int_\Omega \frac{\boldsymbol{u}^k - \boldsymbol{u}^{k-1} + \boldsymbol{u}^{k-2}}{h^2} \cdot (\boldsymbol{u}^k - \boldsymbol{u}^{k-1})\, dx + \int_\Omega \boldsymbol{\sigma}[\boldsymbol{u}^k] : \boldsymbol{\epsilon}[\boldsymbol{u}^k - \boldsymbol{u}^{k-1}]\, dx \\
&\geq \int_\Omega \frac{1}{h^2} (\boldsymbol{u}^k - \boldsymbol{u}^{k-1} - \boldsymbol{u}^{k-1} + \boldsymbol{u}^{k-2}) \cdot (\boldsymbol{u}^k - \boldsymbol{u}^{k-1})\, dx + 2\mu \int_\Omega \frac{\partial u_i^k}{\partial x_j} \frac{\partial (u_i^k - u_i^{k-1})}{\partial x_j}\, dx \\
&\geq \frac{1}{2} \int_\Omega \left(\left| \frac{\boldsymbol{u}^k - \boldsymbol{u}^{k-1}}{h} \right|^2 - \left| \frac{\boldsymbol{u}^{k-1} - \boldsymbol{u}^{k-2}}{h} \right|^2 \right) dx + \mu \int_\Omega \left(\left| \frac{\partial u_i^k}{\partial x_j} \right|^2 - \left| \frac{\partial u_i^{k-1}}{\partial x_j} \right|^2 \right) dx.
\end{aligned}$$

Summing over $k = 1$ to $\ell \leq M$, we obtain

$$\int_\Omega \left(\frac{1}{2} \left| \frac{\boldsymbol{u}^\ell - \boldsymbol{u}^{\ell-1}}{h} \right|^2 + \mu \left| \frac{\partial u_i^\ell}{\partial x_j} \right|^2 \right) dx \leq \int_\Omega \left(\frac{1}{2} \left| \frac{\boldsymbol{u}^0 - \boldsymbol{u}^{-1}}{h} \right|^2 + \mu \left| \frac{\partial u_i^0}{\partial x_j} \right|^2 \right) dx \tag{6.16}$$

Therefore we get

$$\frac{1}{2} \left\| \frac{\partial \widehat{u}_i^h}{\partial t}(t) \right\|_{L^2(\Omega)}^2 + \mu \left\| \frac{\partial \overline{u}_i^h}{\partial x_j}(t) \right\|_{L^2(\Omega)}^2 \leq \frac{1}{2} \left\| v_i^0 \right\|_{L^2(\Omega)}^2 + \mu \left\| \frac{\partial u_i^0}{\partial x_j} \right\|_{L^2(\Omega)}^2 \quad \text{for a.e. } t \in (0, T). \tag{6.17}$$

□

Lemma 3. *Let $\overline{\boldsymbol{u}}^h$ and $\boldsymbol{u}^h$ be defined by* (6.11) *and* (6.12)*. Then the following relations hold.*

$$\left\| \overline{u}_i^h(t) - \widehat{u}_i^h(t) \right\|_{L^2(\Omega)} \leq h \left\| \frac{\partial \widehat{u}_i^h}{\partial t}(t) \right\|_{L^2(\Omega)} \qquad \text{for a.e. } t \in (0, T), \tag{6.18}$$

$$\left\| \frac{\partial \widehat{u}_i^h}{\partial x_j} \right\|_{L^2(Q_T)}^2 \leq \left\| \frac{\partial \overline{u}_i^h}{\partial x_j} \right\|_{L^2(Q_T)}^2 + \frac{h}{2} \left\| \frac{\partial u_i^0}{\partial x_j} \right\|_{L^2(\Omega)}^2 \tag{6.19}$$

Proof. We have

$$
\begin{aligned}
&\left\|\frac{\partial \widehat{u}_i^h}{\partial x_j}\right\|_{L^2(Q_T)}^2 - \left\|\frac{\partial \overline{u}_i^h}{\partial x_j}\right\|_{L^2(Q_T)}^2 \\
&= \int_0^T \int_\Omega \left\{ \left(\frac{\partial \widehat{u}_i^h}{\partial x_j}\right)^2 - \left(\frac{\partial \overline{u}_i^h}{\partial x_j}\right)^2 \right\} dxdt \\
&= \sum_{k=1}^M \int_{(k-1)h}^{kh} \int_\Omega \left\{ \left(\frac{t-(k-1)h}{h}\frac{\partial u_i^k}{\partial x_j} + \frac{kh-t}{h}\frac{\partial u_i^{k-1}}{\partial x_j}\right)^2 + \left(\frac{\partial u_i^k}{\partial x_j}\right)^2 \right\} dxdt \\
&= \sum_{k=1}^M \int_{(k-1)h}^{kh} \int_\Omega \left\{ \frac{(t-(k-1)h)^2 - h^2}{h^2} \left(\frac{\partial u_i^k}{\partial x_j}\right)^2 \right. \\
&\qquad \left. +2\frac{(t-(k-1)h)(kh-t)}{h^2}\frac{\partial u_i^k}{\partial x_j}\frac{\partial u_i^{k-1}}{\partial x_j} + \frac{(kh-t)^2}{h^2}\left(\frac{\partial u_i^{k-1}}{\partial x_j}\right)^2 \right\} dxdt \\
&= \sum_{k=1}^M \int_\Omega \left\{ -\frac{2h}{3}\left(\frac{\partial u_i^k}{\partial x_j}\right)^2 + \frac{h}{3}\frac{\partial u_i^k}{\partial x_j}\frac{\partial u_i^{k-1}}{\partial x_j} + \frac{h}{3}\left(\frac{\partial u_i^{k-1}}{\partial x_j}\right)^2 \right\} dx \\
&\le \frac{h}{6}\sum_{k=1}^M \int_\Omega \left\{ -4\left(\frac{\partial u_i^k}{\partial x_j}\right)^2 + \left(\frac{\partial u_i^k}{\partial x_j}\right)^2 + \left(\frac{\partial u_i^{k-1}}{\partial x_j}\right)^2 + 2\left(\frac{\partial u_i^{k-1}}{\partial x_j}\right)^2 \right\} dx \\
&= \frac{h}{2}\sum_{k=1}^M \int_\Omega \left\{ -\left(\frac{\partial u_i^k}{\partial x_j}\right)^2 + \left(\frac{\partial u_i^{k-1}}{\partial x_j}\right)^2 \right\} dx \\
&= \frac{h}{2}\int_\Omega \left\{ -\left(\frac{\partial u_i^M}{\partial x_j}\right)^2 + \left(\frac{\partial u_i^0}{\partial x_j}\right)^2 \right\} dx \\
&\le \frac{h}{2}\left\|\frac{\partial u_i^0}{\partial x_j}\right\|_{L^2(\Omega)}^2 .
\end{aligned}
$$

Let $t \in ((k-1)h, kh)$. Then we obtain

$$
\begin{aligned}
\left\|\overline{u}_i^h(t) - \widehat{u}_i^h(t)\right\|_{L^2(\Omega)}^2 &= \int_\Omega \left(u_i^k - \frac{t-(k-1)h}{h}u_i^k - \frac{kh-t}{h}u_i^{k-1}\right)^2 dx \\
&= \int_\Omega \left(\frac{kh-t}{h}\right)^2 \left(u_i^k - u_i^{k-1}\right)^2 dx \\
&\le \int_\Omega \left(u_i^k - u_i^{k-1}\right)^2 dx \\
&= h^2 \int_\Omega \left(\frac{\partial \widehat{u}_i^h}{\partial t}(t)\right)^2 dx.
\end{aligned}
$$

□

Theorem 5. *Suppose Ω is a bounded domain with smooth boundary. Then a limit function*

$\boldsymbol{u}$ belongs to $W^{1,2}(Q_T;\mathbb{R}^d)$ and satisfies

$$\int_0^T \int_\Omega \left(-\frac{\partial \boldsymbol{u}}{\partial t} \cdot \frac{\partial \boldsymbol{w}}{\partial t} + \boldsymbol{\sigma}[\boldsymbol{u}] : \boldsymbol{\epsilon}[\boldsymbol{w}] \right) dx\, dt - \int_\Omega \boldsymbol{v}^0 \cdot \boldsymbol{w}(0,\boldsymbol{x})\, dx = 0 \tag{6.20}$$

for all $\boldsymbol{w} \in C_0^\infty([0,T)\times\Omega;\mathbb{R}^d)$. We call $\boldsymbol{u}$ a weak solution.

Proof. Using (6.15), we can apply the theorem by Eberlein and Shmulyan to construct a subsequence $\{\frac{\partial \overline{u}_i^{h_\ell}}{\partial x_j}\}_{\ell\in\mathbb{N}}$ converging weakly in $L^2(Q_T)$ to a function v_{ij}. From the sequence $\{h_\ell\}_{\ell\in\mathbb{N}}$, we construct another subsequence $\{h_{\ell_r}\}_{r\in\mathbb{N}}$ such that $\{\frac{\partial \widehat{u}_i^{h_{\ell_r}}}{\partial t}\}_{r\in\mathbb{N}}$ converges weakly in $L^2(Q_T)$ to a function U_i. We omit this lengthy explanation and subscripts and simply write

$$\frac{\partial \overline{u}_i^h}{\partial x_j} \rightharpoonup \mathrm{v}_{ij} \quad \text{in } L^2(Q_T), \tag{6.21}$$

$$\frac{\partial \widehat{u}_i^h}{\partial t} \rightharpoonup U_i \quad \text{in } L^2(Q_T). \tag{6.22}$$

From Poincaré's inequality we know that there is a constant C_P so that

$$\left\|\widehat{u}_i^h\right\|_{L^2(Q_T)} \le C_P \left\| \frac{\partial \widehat{u}_i^h}{\partial x_j} \right\|_{L^2(Q_T)}. \tag{6.23}$$

Now, (6.15), (6.18) and (6.23) imply that $\widehat{u}_i^h$ is uniformly bounded in $W^{1,2}(Q_T)$. Therefore, there is a weakly convergent subsequence in $W^{1,2}(Q_T)$ and, by Rellich theorem, a strongly converging subsequence in $L^2(Q_T)$. Let us denote the cluster function as u_i:

$$\widehat{u}_i^h \rightharpoonup u_i \quad \text{in } W^{1,2}(Q_T). \tag{6.24}$$

Because of (6.22), $U_i = \frac{\partial u_i}{\partial t}$ holds almost everywhere. Moreover, from (6.21), for any $w \in C_0^\infty(Q_T)$

$$\int_0^T \int_\Omega \left(\frac{\partial \overline{u}_i^h}{\partial x_j} - \frac{\partial \widehat{u}_i^h}{\partial x_j} \right) w\, dxdt \to \int_0^T \int_\Omega \left(\mathrm{v}_{ij} - \frac{\partial u_i}{\partial x_j} \right) w\, dxdt \quad \text{as } h \to 0+, \tag{6.25}$$

while at the same time

$$\int_0^T \int_\Omega \left(\frac{\partial \overline{u}_i^h}{\partial x_j} - \frac{\partial \widehat{u}_i^h}{\partial x_j} \right) w\, dxdt = -\int_0^T \int_\Omega \left(\overline{u}_i^h - \widehat{u}_i^h \right) \frac{\partial w}{\partial x_j}\, dxdt \to 0 \quad \text{as } h \to 0+, \tag{6.26}$$

by (6.19). This means that $\mathrm{v}_{ij} = \frac{\partial u_i}{\partial x_j}$ almost everywhere in Q_T.

We have shown in this way that there is a function $u_i \in W^{1,2}(Q_T)$, such that

$$\frac{\partial \overline{u}_i^h}{\partial x_j} \rightharpoonup \frac{\partial u_i}{\partial x_j} \quad \text{in } L^2(Q_T) \tag{6.27}$$

$$\frac{\partial \widehat{u}_i^h}{\partial t} \rightharpoonup \frac{\partial u_i}{\partial t} \quad \text{in } L^2(Q_T). \tag{6.28}$$

The relation (6.13) holds also when multiplied by any function $\widetilde{w} \in C([0,T])$. Hence, integrating over the time interval $(0,T)$ and using a standard density argument, we arrive at

$$\int_0^T \int_\Omega \left\{ \frac{1}{h} \left(\frac{\partial \widehat{\boldsymbol{u}}^h}{\partial t}(t) - \frac{\partial \widehat{\boldsymbol{u}}^h}{\partial t}(t-h) \right) \cdot \boldsymbol{w} + \boldsymbol{\sigma}[\overline{\boldsymbol{u}}^h] : \boldsymbol{\epsilon}[\boldsymbol{w}] \right\} dx = 0 \tag{6.29}$$

for all $\boldsymbol{w} \in L^2(0,T; W_0^{1,2}(\Omega;\mathbb{R}^d))$. Now, we can pass to limit in (6.29) as $h \to 0+$. We shall, for the time being, consider a test function $\boldsymbol{w}$ belonging to $C_0^\infty([0,T)\times\Omega)$. To begin with, we have

$$\begin{aligned}
\int_0^T \int_\Omega \boldsymbol{\sigma}[\overline{\boldsymbol{u}}^h] : \boldsymbol{\epsilon}[\boldsymbol{w}]\, dxdt &= \int_0^T \int_\Omega c_{ijpq} \frac{\partial \overline{u}_p^h}{\partial x_q} \frac{\partial w_i}{\partial x_j}\, dxdt \\
&\to \int_0^T \int_\Omega c_{ijpq} \frac{\partial u_p}{\partial x_q} \frac{\partial w_i}{\partial x_j}\, dxdt \quad \text{as } h \to 0 \\
&= \int_0^T \int_\Omega \boldsymbol{\sigma}[\boldsymbol{u}] : \boldsymbol{\epsilon}[\boldsymbol{w}]\, dxdt.
\end{aligned}$$

Moreover, we have

$$\begin{aligned}
&\int_0^T \int_\Omega \frac{1}{h} \left\{ \frac{\partial \widehat{\boldsymbol{u}}^h}{\partial t}(t) - \frac{\partial \widehat{\boldsymbol{u}}^h}{\partial t}(t-h) \right\} \cdot \boldsymbol{w}(t)\, dxdt \\
&= \int_0^T \int_\Omega \frac{1}{h} \frac{\partial \widehat{\boldsymbol{u}}^h}{\partial t}(t) \cdot \boldsymbol{w}(t)\, dxdt - \int_{-h}^{T-h} \int_\Omega \frac{1}{h} \frac{\partial \widehat{\boldsymbol{u}}^h}{\partial t}(t) \cdot \boldsymbol{w}(t+h)\, dxdt \\
&= -\int_0^T \int_\Omega \frac{\partial \widehat{\boldsymbol{u}}^h}{\partial t}(t) \cdot \frac{\boldsymbol{w}(t+h) - \boldsymbol{w}(t)}{h}\, dxdt - \int_{-h}^0 \int_\Omega \frac{1}{h} \frac{\partial \widehat{\boldsymbol{u}}^h}{\partial t}(t) \cdot \boldsymbol{w}(t+h)\, dxdt \\
&\quad + \int_{T-h}^T \int_\Omega \frac{1}{h} \frac{\partial \widehat{\boldsymbol{u}}^h}{\partial t}(t) \cdot \boldsymbol{w}(t+h)\, dxdt
\end{aligned} \tag{6.30}$$

For the first therm of (6.30), we have

$$-\int_0^T \int_\Omega \frac{\partial \widehat{\boldsymbol{u}}^h}{\partial t}(t) \cdot \frac{\boldsymbol{w}(t+h) - \boldsymbol{w}(t)}{h}\, dxdt \to -\int_0^T \int_\Omega \frac{\partial \boldsymbol{u}}{\partial t} \cdot \frac{\partial \boldsymbol{w}}{\partial t}\, dxdt \quad \text{as } h \to 0+.$$

For the second term of (6.30), since $\frac{\partial \widehat{\boldsymbol{u}}^h}{\partial t}(t) = (\boldsymbol{u}^0 - \boldsymbol{u}^{-1})/h = \boldsymbol{v}_0$ for $t \in (-h, 0)$ we have

$$-\int_{-h}^0 \int_\Omega \frac{1}{h} \frac{\partial \widehat{\boldsymbol{u}}^h}{\partial t}(t) \cdot \boldsymbol{w}(t+h)\, dxdt \to -\int_\Omega \boldsymbol{v}_0 \cdot \boldsymbol{w}(\boldsymbol{x}, 0)\, dx \quad \text{as } h \to 0+.$$

For the third term of (6.30), since $\boldsymbol{w}(t+h) = 0$ for $t \in (T-h, T)$ we obtain

$$\int_{T-h}^T \int_\Omega \frac{1}{h} \frac{\partial \widehat{\boldsymbol{u}}^h}{\partial t}(t) \cdot \boldsymbol{w}(t+h)\, dxdt \to 0 \quad \text{as } h \to 0+.$$

Thus, we can finally state (6.20). □

Chapter 7

Conclusion

In the thesis we attempt to study a dynamical rolling contact problem based on a variational method, starting from the derivation of suitable model equations, developing numerical scheme and obtaining numerical results.

Decomposing deformation into rotation and small displacement, we described dynamical rolling contact problem as a linear elasticity problem with outer force coming from rotation. We were not able to proof the existence of weak solutions of the problem. We proved the existence of minimizers for the time-discrete minimization problem by the general theory. We proposed the numerical scheme which preserves the discretized total energy and a variant of nonlinear conjugate gradient method which is possible to treat constraint. The proposed time discrete scheme haves $O(\Delta t^2)$–accuracy for the acceleration part, but the oder of the approximation of the outer force is $O(\Delta t)$. We need further consideration. Based on these numerical results, the proposed method shows promise to help with the understanding of the source of the squeaking sound in a scanner's roller.

The investigation of dynamical contact problem is not closed. To achieve the goal that analyze the squeaking sound, it is necessary to further improve the model. We consider the resonance coming from the interactions of contact between rubber roller and paper is important. For example, friction and adhesion force are candidate as such interactions. An implementation that includes the stick-slip friction force at the contact is under development.

Acknowledgements

First, I would like to thank my supervisor, professor Seiro Omata who has been giving me a number of invaluable supports and advices. Thanks to him I learned about the very interesting fields of mathematics. The author cannot finish this work without his help.

I would like to thank professor Norbert Pozar and Dr. Patrick van Meurs for their valuable advice and kindness in many ways. Their approach to mathematics has highly inspired me.

I am grateful for advice, help and encouragement of professors Masato Kimura, Hiroshi Ohtsuka, Kenichi Nakamura, Hirofumi Notsu and Katsuyoshi Ohara.

I also would like to thank my advisor professor Takeshi Fukao who made go to Kanazawa possible.

I would like to thank all of my schoolmates, especially to Dr.Vu Thi Thu Giang, and Dr.Reza Rendian Septiawan who was helping me.

Bibliography

[1] Y.Akagawa, S.Morikawa, S.Omata, *A numerical approach based on variational methods to an elastodynamic contact problem*, To be submitted in Sci. Rep. Kanazawa Univ..

[2] G.Ambati, J.F.W.Bell, J.C.K.Sharp, *In-Plane Vibrations of Annular Rings*, Journal of Sound and Vibration **47**(3), 1976, 415–432.

[3] H.Brezis, *Functional Analysis, Sobolev Spaces and Partial Differential Equations*, Springer, 2010.

[4] R.Bridson, *Fast Poisson Disk Sampling in Arbitrary Dimensions*, ACM SIGGRAPH 2007 sketches Article No. 22, 2007.

[5] J.Cea, *Lectures on Optimization –Theory and Algorithms*, Tata Institute of Fundamental Research, Bombay.

[6] P.G.Ciarlet, *Three-Dimensional Elasticity*, Elsevier, 1994.

[7] D.Dunbar, G.Humphreys, *A spatial data structure for fast Poisson-disk sample generation*, ACM Trans. Graph. **25** (3), 2006, 503–508.

[8] L.C.Evans, *Partial Differential Equations*, Graduate Studies in Mathematics, AMS, Providence, Rhode Island, 1998.

[9] I.Hlaváček, J.Haslinger, J.Nečas, J.Lovíšek, *Solution of Variational Inequalities in Mechanics*, Springer, New York (1988)

[10] G.Hu, P.Wriggers, *On the adaptive finite element method of steady-state rolling contact for hyperelasticity in finite deformations*, Comput. Methods Appl. Mech. Engrg. **191** (2002), 1333–1348.

[11] H.Imai, K.Kikuchi, K.Nakane, S.Omata, T.Tachikawa, *A numerical approach to the asymptotic behavior of solutions of a one-dimensional hyperbolic free boundary problem*, JJIAM **18** (1), 2001, pp. 43-58.

[12] K.Ito, M.Kazama, H.Nakagawa, K.Švadlenka, *Numerical solution of a volume- constrained free boundary problem by the discrete Morse flow method*, accepted to Gakuto International Series, Proceedings of the International Conference on Free Boundary Problems in Chiba 2007.

[13] N.Kikuchi, *An approach to the construction of Morse flows for variational functionals*, Nematics - Mathematical and Physical Aspects, Nato Adv. Sci. Inst. Ser. C: Math. Phys. Sci. **332**, Kluwer Acad. Publ., Dodrecht-Boston-London (1991), 195–198.

[14] K.Kikuchi, *Constructing a solution in time semidiscretization method to an equation of vibrating string with an obstacle*, preprint.

[15] K.Kikuchi, S.Omata, *A free boundary problem for a one dimensional hyperbolic equation*, Adv. Math. Sci. Appl. **9** (2), 1999, pp. 775-786.

[16] N.Kikuchi, J.T.Oden, *Contact Problems in Elasticity: A Study of Variational Inequalities and Finite Element Methods*, SIAM, Philadelphia (1988).

[17] T.A.Laursen, *Computational Contact and Impact Mechanics*, Springer-Verlag, New York (2002).

[18] J.L.Lions, G.Stampacchia, *Variational inequalities*, Commun. Pure Appl. Math. **20**, (1967), 493–519.

[19] T.Nagasawa, S.Omata, *Discrete Morse semiflows of a functional with free boundary*, Adv. Math. Sci. Appl. **2** (1), 1993, pp. 147-187.

[20] T.Nagasawa, K.Nakane, S.Omata, *Numerical computations for motion of vortices governed by a hyperbolic Ginzburg-Landau System*, Nonlinear Anal. **51** (1), Ser A: Theory Methods, 2002, pp. 67–77.

[21] J.T.Oden, T.L.Lin, *On the general rolling contact problem for finite deformations of a viscoelastic cylinder*, Comput. Methods Appl. Mech. Engrg. (1986), 297–367.

[22] S.Omata, *A numerical method based on the discrete Morse semiflow related to parabolic and hyperbolic equations*, Nonlinear Analysis **30** (4), 1997, pp. 2181-2187.

[23] S.Omata, *A Numerical treatment of film motion with free boundary*, Adv. Math. Sci. Appl. **14**, 2004, pp. 129-137.

[24] S.Omata, T.Okamura, K.Nakane, *Numerical analysis for the discrete Morse semi- flow related to Ginzburg Landau functional*, Nonlinear Analysis **37** (5), 1999, pp. 589-602.

[25] J.R.Shewchuk, *Delaunay Mesh Generation*, Chapter 2, Lecture Notes at Department of Electrical Engineering and Computer Sciences, University of California at Berkeley, CA 94720 on February 5, 2012.

[26] A.Signorini, *Sopra alcune questioni di statica dei sistemi continui*, Annali della Scuola Normale Superiore di Pisa **2**, (1933), 231–251.

[27] K.Švadlenka, S.Omata, *Construction of solutions to heat-type problems with volume constraint via the discrete Morse flow*, Funkc. Ekvac. **50**, 2007, pp. 261-285.

[28] K.Švadlenka, S.Omata, *Mathematical modelling of surface vibration with volume constraint and its analysis*, Nonlinear Analysis, **69** (9), 2008, 3202–3212.

[29] K.Švadlenka, S.Omata, *Mathematical analysis of a constrained parabolic free boundary problem describing droplet motion on a surface*, Indiana University Mathematics Journal **58** (5), 2009, pp. 2073–2102.

[30] A.Tachikawa, *A variational approach to constructing weak solutions of semilinear hyperbolic systems*, Adv. Math. Sci. Appl. **4**, (1994), 93–103.

[31] T.Yamazaki, S.Omata, K.Švadlenka, K.Ohara, *Construction of approximate solu- tion to a hyperbolic free boundary problem with volume constraint and its numerical computation*, Adv. Math. Sci. Appl. **16** (1), 2006, pp. 57–67.